Artwork by Marisa Petrusky

Where do Neutrons Go?

Dr. Rakitha Beminiwattha

For the PREX Collaboration

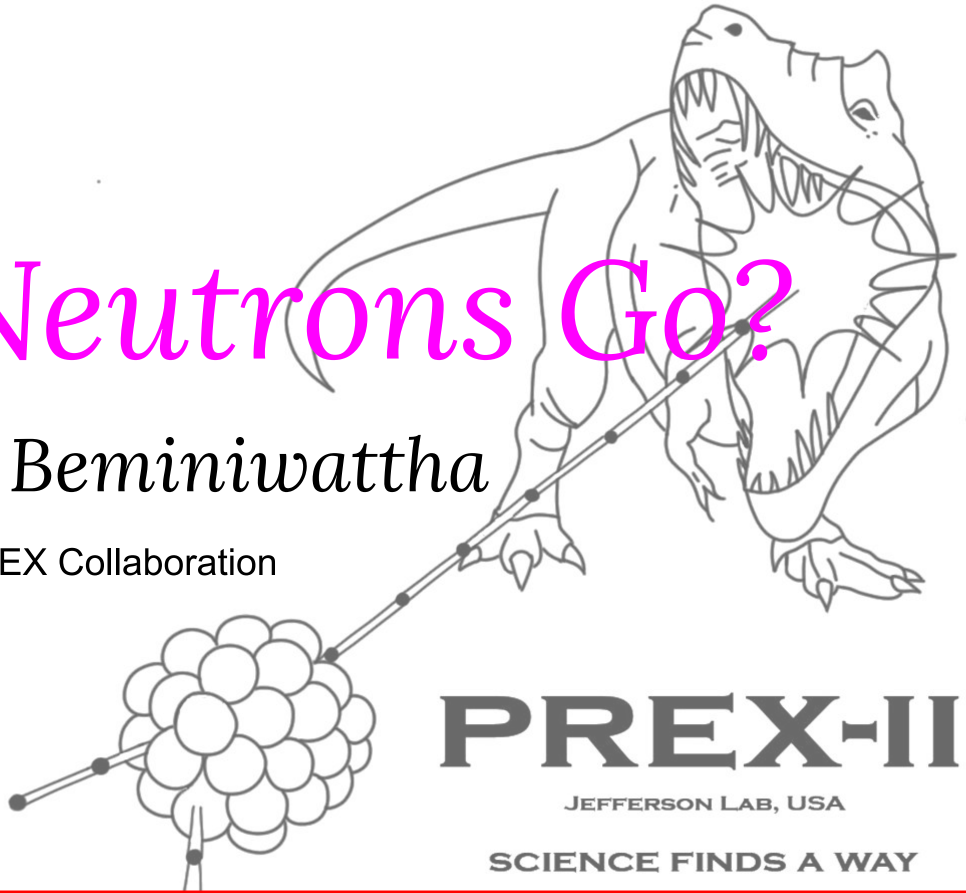

Ohio University Physics INPP Seminar
November 23rd, 2021

Louisiana Tech University
College of Science and Engineering

Where do Neutrons Go?

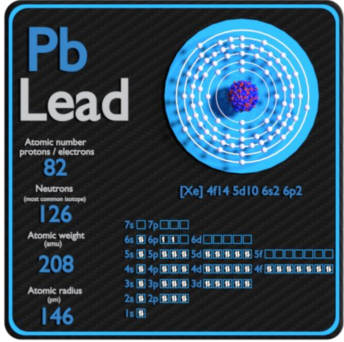

Consider the heaviest known doubly magic nucleus, lead-208 (^{208}Pb) that has 82 protons and 126 neutrons

The Coulomb repulsion among its protons leads to a large neutron excess

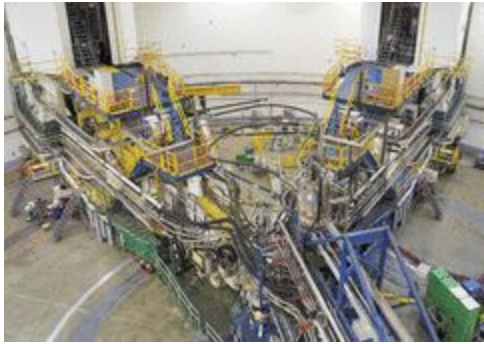

Where do these excess Neutrons in Nucleus go?

The **P**b **R**adius **EX**periment (PREX), at the JLab was built to measure the location of these excess neutrons

Answer to this simple question help us understand the structure of both atomic nuclei and neutron stars.

^{208}Pb

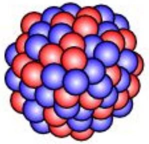

separated by 18 orders of magnitude in size

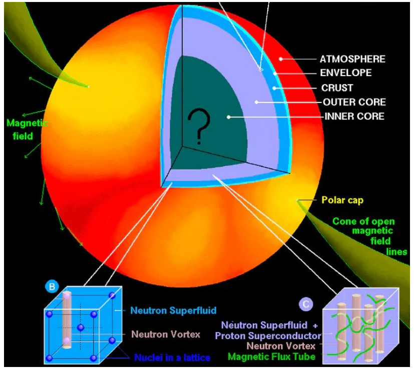

Where do Neutrons in Nucleus go?

PREX was designed to measure the first model-independent **rms radius** of the neutron distribution in ^{208}Pb

The difference between rms radii of proton distribution and neutron distribution is known as the **neutron-skin thickness**, a region in nucleus appear to be populated primarily by neutrons

There is a strong correlation between the **neutron-skin thickness** of heavy nuclei such as ^{208}Pb and the **radius of a neutron star**

This correlation can be better understand by using the liquid-drop model

Thiel et al J.Phys.G 46 (2019) 9, 093003

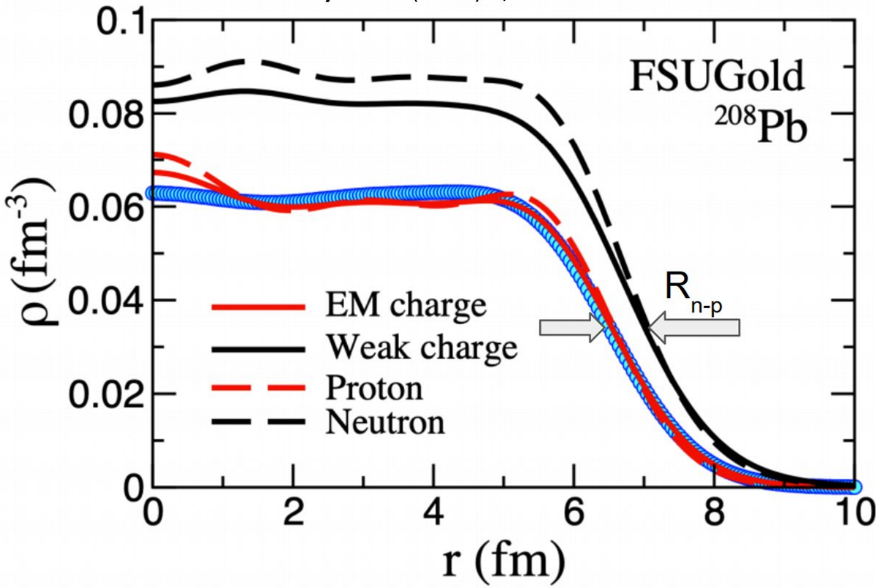

Liquid Drop Model

wikipedia

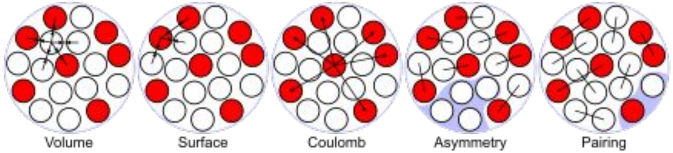

$$E_B = a_V A - a_S A^{2/3} - a_C \frac{Z(Z-1)}{A^{1/3}} - a_A \frac{(N-Z)^2}{A} + \delta(N,Z)$$

- In the liquid drop model, the atomic nucleus is regarded as an **incompressible drop consisting of two quantum fluids**. One is electrically charged and consists of Z protons; the other is electrically neutral with N neutrons.
- The radius of the proton distribution (charged drop) has been accurately measured going back to the 1950s.
- The neutron distribution comes entirely from experiments involving strongly interacting probes, such as pions and protons. Strong probes are difficult to decode because of myriad theoretical uncertainties.
- The **symmetry energy** a_A term and its density dependence is the link between the **neutron-skin thickness** of a nuclei to the **radius of a neutron star**
- The semi empirical mass formula does not provide density dependance of liquid drop
- The density dependent information comes from the **equation of state** (**EOS**) which states the energy of the system depends on the density and neutron–proton asymmetry of the system

Equation of State (EOS)

The density dependent information comes from the equation of state (EOS) which states the energy of the system depends on the density and neutron–proton asymmetry of the system

$$\frac{E}{A} - m = \mathcal{E}(\rho,\alpha) = \mathcal{E}_{SNM}(\rho) + \alpha^2 S(\rho) + \mathcal{O}(\alpha^4)$$

$$S(\rho) = J + L\left(\frac{\rho - \rho_0}{3\rho_0}\right) + \cdots \qquad L = 3\rho_0 \frac{\partial S}{\partial \rho}\bigg|_{\rho=\rho_0}$$

The term **density dependent symmetry energy** or **symmetry pressure (L)**

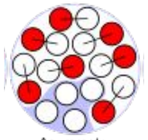

Both the neutron-skin thickness of atomic nuclei and the radius of a neutron star are related to this term, symmetry pressure (L) *

* C. J. Horowitz et al., *J. Phys.* G **41**, 093001 (2014). https://doi.org/10.1088/0954-3899/41/9/093001

Different Systems, Same EOS

Stiff EOS -> larger pressure for a given density. Resists compression and larger radii. **Soft EOS** -> smaller pressures, compressible, and smaller radii

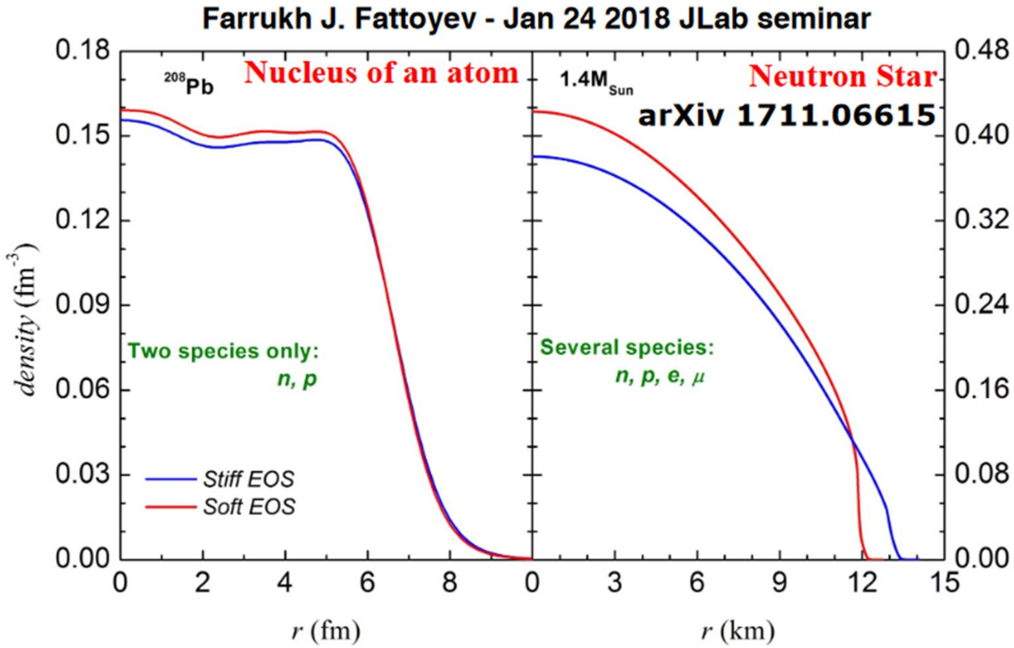

While the ^{208}Pb nucleus and a neutron star are separated by 18 orders of magnitude in size they are believed to be made out of the same matter and obey the equation of state (EOS)

Parity Violating Electron Scattering

- Due to parity violating (PV) nature of the neutral current, the differential cross section is dependent on the helicity of the electron
- The difference in helicity correlated scattering cross section is known as the PV asymmetry
- Detectable (10^{-6}) PV asymmetry is produced

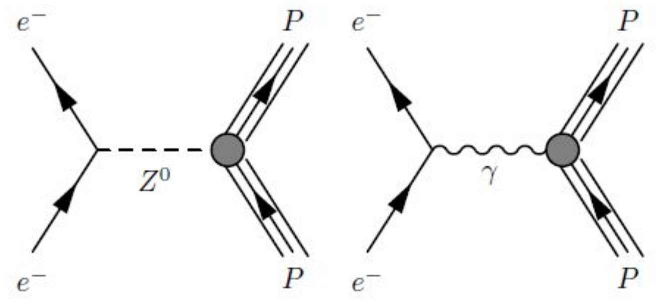

Differential scattering cross section,

$$\frac{\mathrm{d}\sigma}{\mathrm{d}\Omega} \propto |\mathrm{M}^{\mathrm{Total}}|^2 \simeq |\mathrm{M}^{\mathrm{EM}}|^2$$

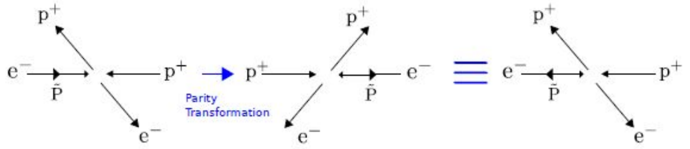

$$\mathrm{A_{LR}} = \frac{\frac{\mathrm{d}\sigma^{\mathrm{R}}}{\mathrm{d}\Omega} - \frac{\mathrm{d}\sigma^{\mathrm{L}}}{\mathrm{d}\Omega}}{\frac{\mathrm{d}\sigma^{\mathrm{R}}}{\mathrm{d}\Omega} + \frac{\mathrm{d}\sigma^{\mathrm{L}}}{\mathrm{d}\Omega}} \propto \frac{\mathrm{M}^{\mathrm{EM}} \cdot \mathrm{M}^{\mathrm{NC}}}{|\mathrm{M}^{\mathrm{EM}}|^2}$$

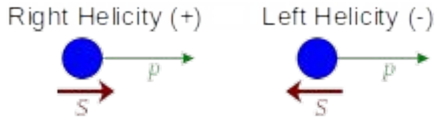

In Born approx. $Q^2 << M^2_Z$

gamma-z interference

$$A_{\mathrm{PV}} = \frac{\sigma^+ - \sigma^-}{\sigma^+ + \sigma^-} = \frac{G_F Q^2}{4\pi\alpha\sqrt{2}}\left[1 - 4\sin^2\theta_W - \frac{F_n(Q^2)}{F_p(Q^2)}\right]$$

$$Q_{\mathrm{weak}}^{\mathrm{proton}} \propto 1 - 4\sin^2\theta_{\mathrm{W}} \approx 0.076, \quad Q_{\mathrm{weak}}^{\mathrm{neutron}} \approx -1$$

Neutral Current as a Probe of the Neutron

Weak neutral current : A clean probe couples mainly to neutrons

$$A_{PV} = \frac{\frac{d\sigma^R}{d\Omega} - \frac{d\sigma^L}{d\Omega}}{\frac{d\sigma^R}{d\Omega} + \frac{d\sigma^L}{d\Omega}} \approx \frac{G_F Q^2}{4\pi\alpha\sqrt{2}} \frac{Q_W F_W(Q^2)}{Z F_{ch}(Q^2)} \rightarrow 10^{-6}$$

$$Q^n_{weak} \sim -1$$

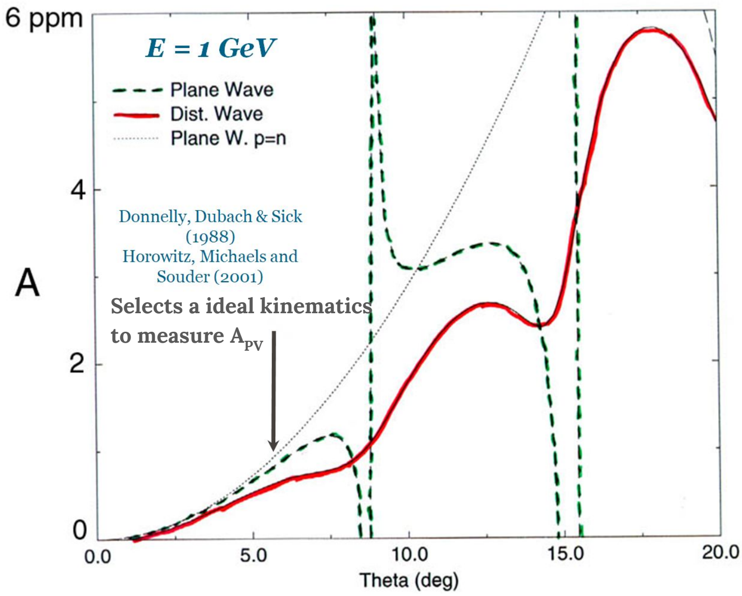

It provides theoretically clean method to measure neutron radius and skin thickness

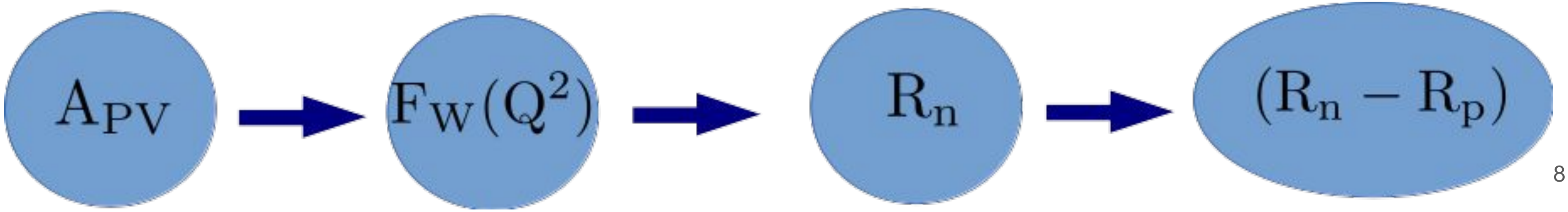

Weak Charge Distribution of ^{208}Pb

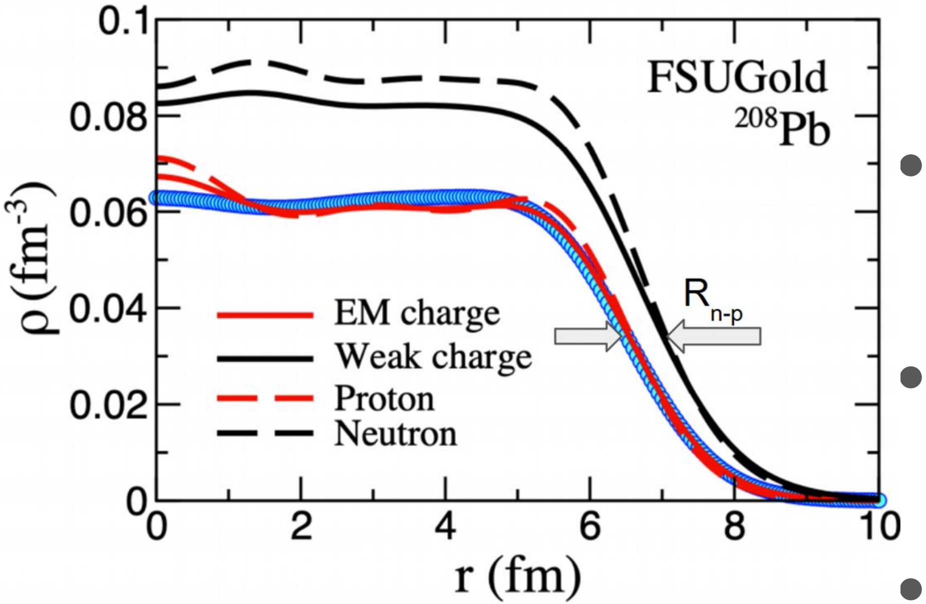

- A clean measurement of neutron skin R_{n-p} will constraint nuclear theory predictions of R_{n-p}
- Neutron skin thickness is highly sensitive to the pressure in neutron-rich matter
- The greater the pressure, the thicker the skin as neutrons are pushed out against surface tension
- ^{208}Pb is well suited to this study: large, uniform, doubly magic

Experimental Overview

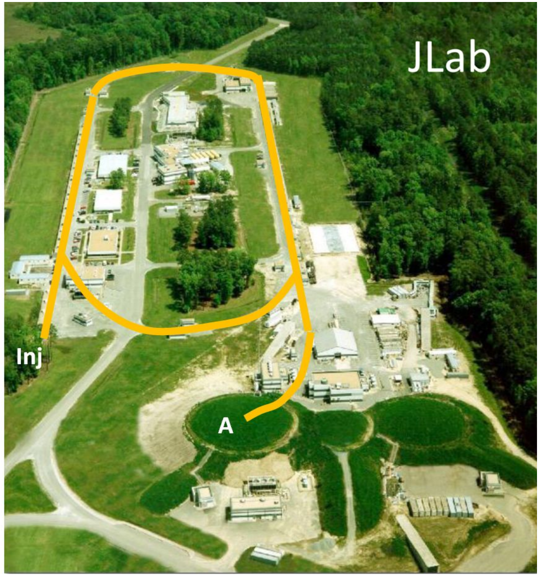

CEBAF is the ONLY operating facility in the world where such an experiment could be attempted
Experimental Challenges: polarized beam, small asymmetry, false beam asymmetries, high electrons rates, radiation load, inelastic and transverse background

Beam Preparation

Double Wien allowed us to further electromagnetically flip the electron beam helicity every few weeks

Beam monitors allowed for injector setup with small beam asymmetries

Mott polarimeter confirm high beam polarization

Injector laser setup crucial towards minimizing beam asymmetries

Pockels cell allowed us to flip the electron helicity at 120 or 240 Hz

Half Wave Plate allowed us to independently flip the laser polarization every few hours

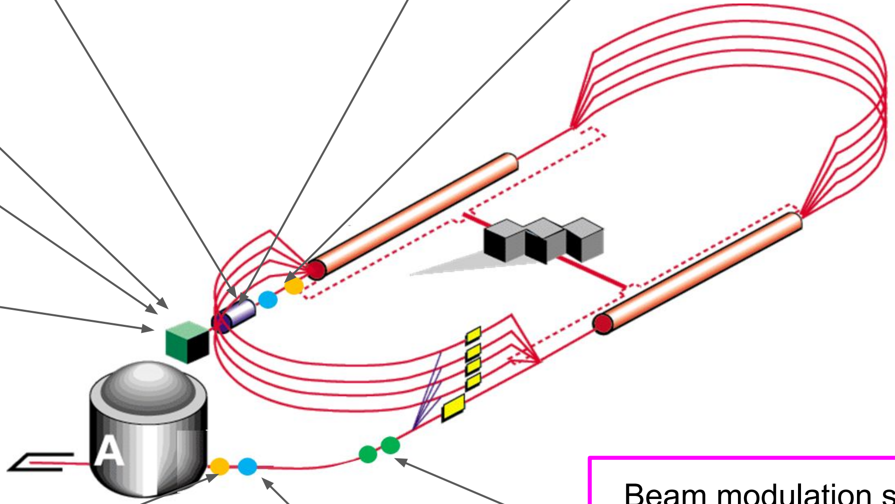

Beam modulation system allows us to span the phase space of beam motion

Beam monitors allow us to determine beam properties in front of the target

Polarimeters allow us to monitor polarization and check machine setup

Polarized Electron Source

- The GaAs strained cathode photo emits selected **helicity** electrons excited by a circularly polarized laser
- It also acts as an “analyzer” with a preferred axis for linear polarization
- The system relies on a Pockels Cell to produce quick changes between opposite circular polarization states
- Imperfections between the two polarization states will lead to beam asymmetries
    - Careful setup and constant monitoring is needed to mitigate any changes in the accelerator setup that introduce such asymmetries

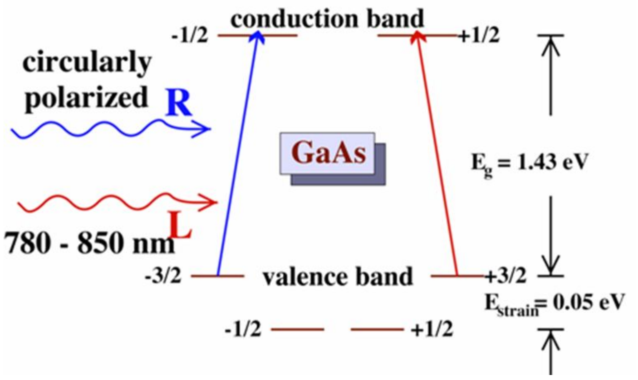

New UVa RTP cell

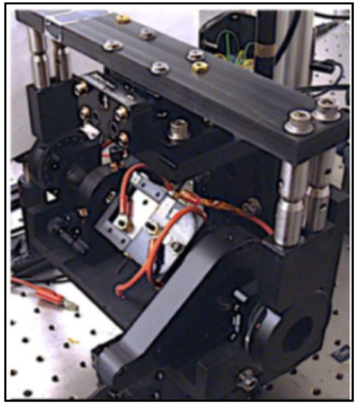

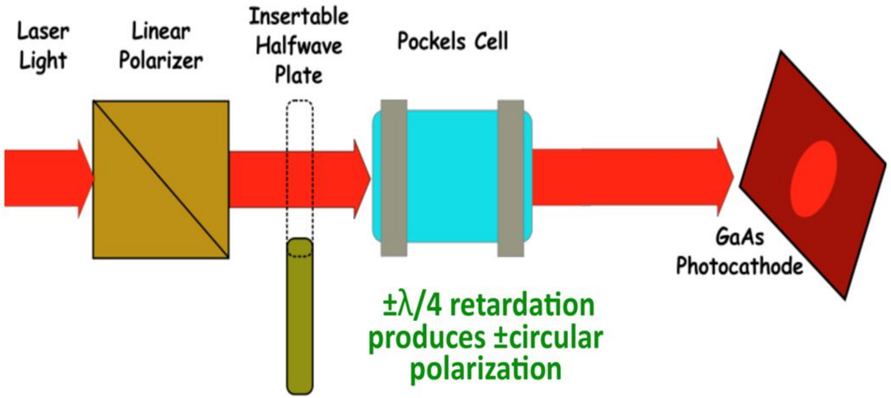

Slow Reversal of Helicity

- A **Pockels Cell** to produce quick changes between opposite circular polarization states
- **Insertable Halfwave Plate**: reverses polarization of the laser light
- The "**double Wien**" manipulates spin - allows us to reverse the polarization of the electron beam
- These flips act to both identify, and cancel, potential beam related asymmetries

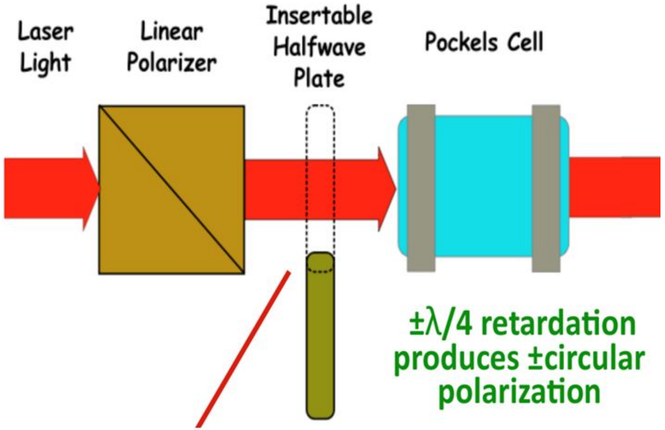

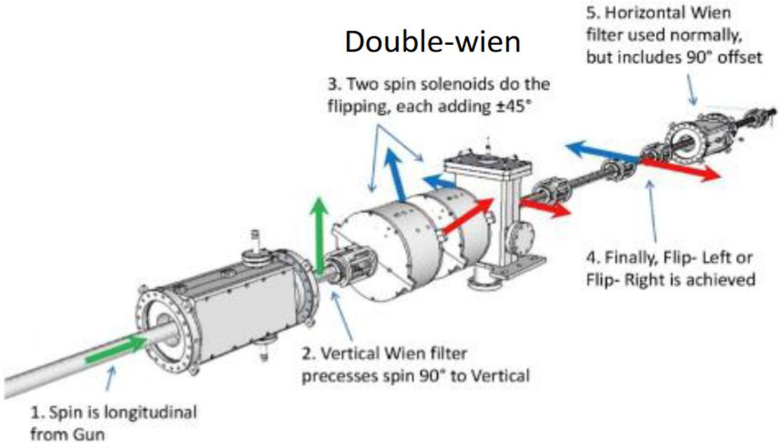

Electron Beam Polarimetry: Moller Polarimeter

- Low-current, invasive measurement
- 4 T field provides saturated magnetization perpendicular to the foil
- Polarimeter runs were taken approximately every week and established no significant fluctuations in beam polarization over the course of the run

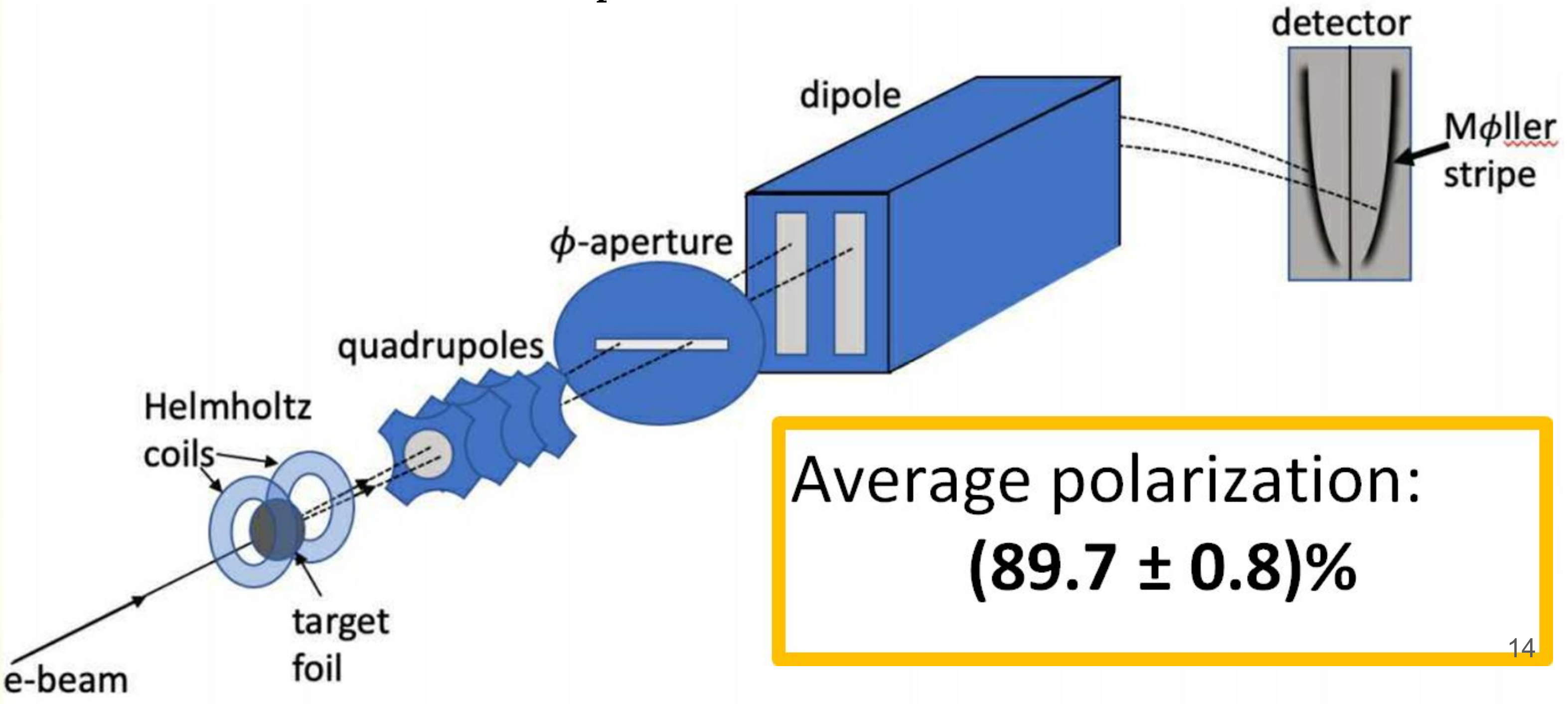

Average polarization:
(89.7 ± 0.8)%

Electron Beam Polarimetry: Moller Polarimeter

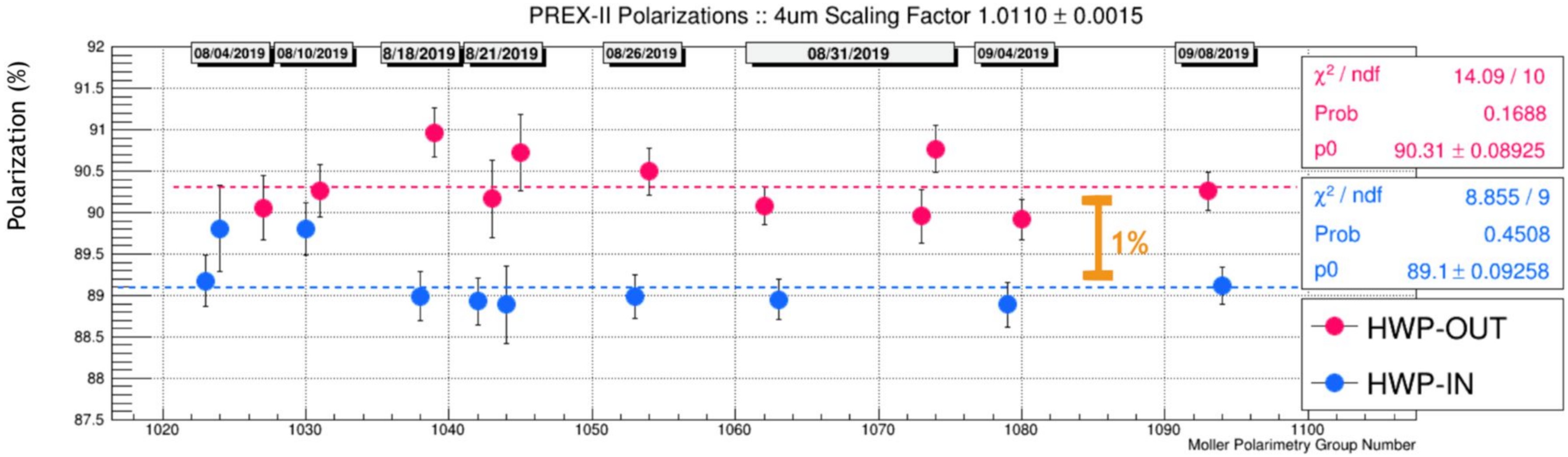

Average polarization:
(89.7 ± 0.8)%

High Resolution Spectrometer (HRS)

- Spectrometer separates elastic peak, directs it onto integrating detector
- Integrate detector in each of the spectrometer pair

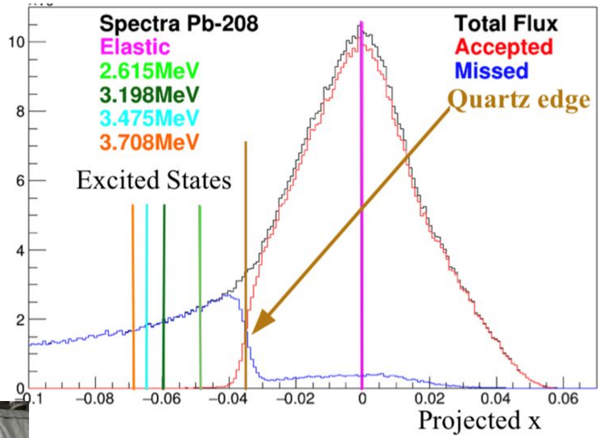

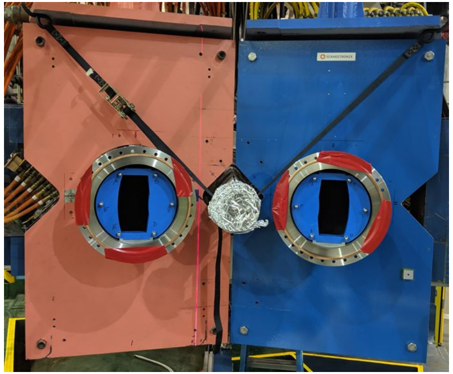

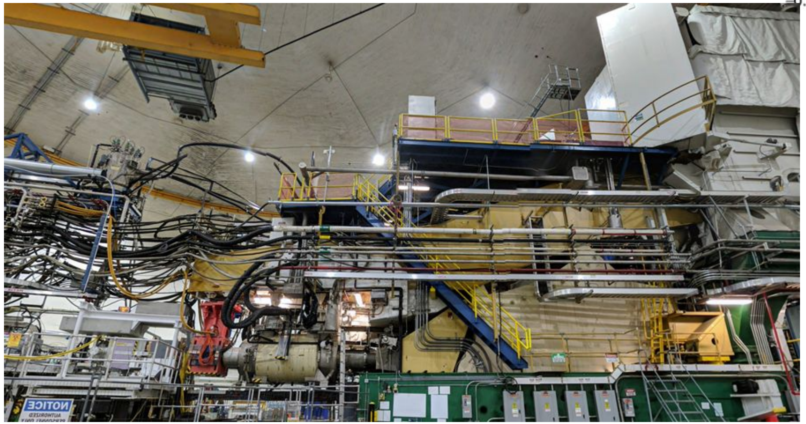

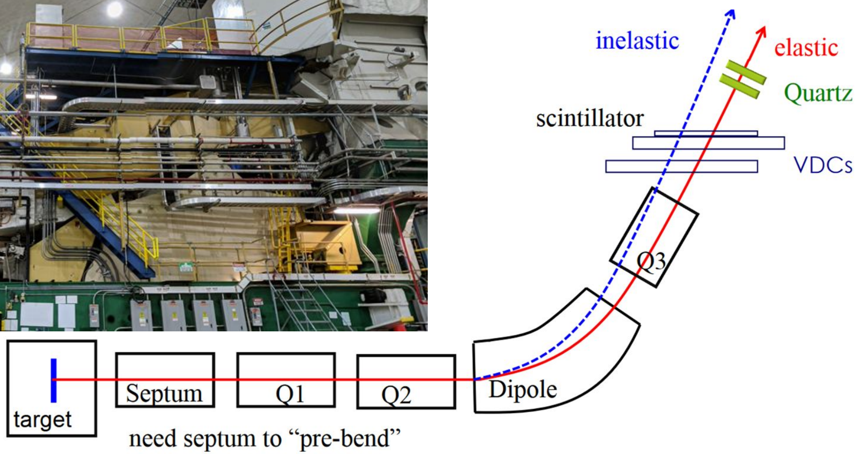

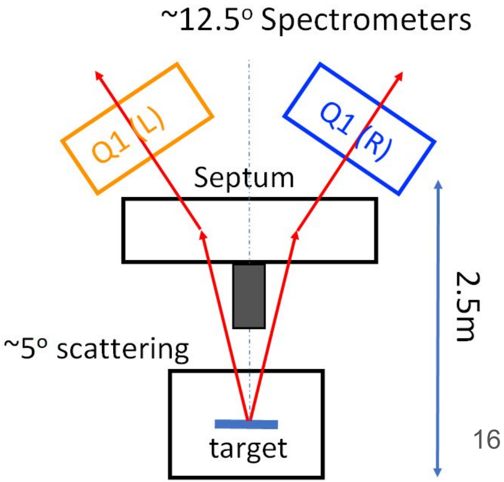

Radiation Shielding

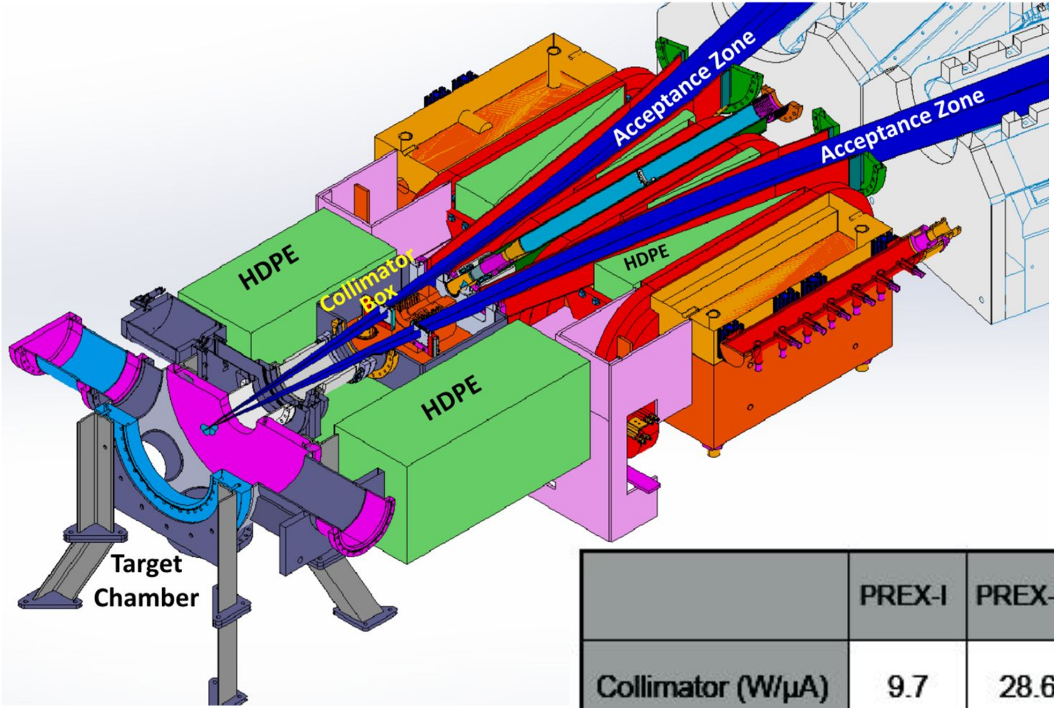

	PREX-I	PREX-II	CREX
Collimator (W/µA)	9.7	28.6	5.2
Hall (W/µA)	18.0	3.4	0.6

- Unique challenges for a high luminosity, high Z, low energy experiment
- Large angle scattered electrons need to be stopped close to the target and that region needs to be heavily shielded
- Electronics inside the hall need to be protected from both the electromagnetic and neutron radiation damage that will stop it from functioning properly

Radiation Shielding

- 2.5 kW power in **collimator** at 70 uA
- Concrete and plastic around collimator region
- Concrete above to stop up-going neutrons creating “skyshine” boundary dose rates

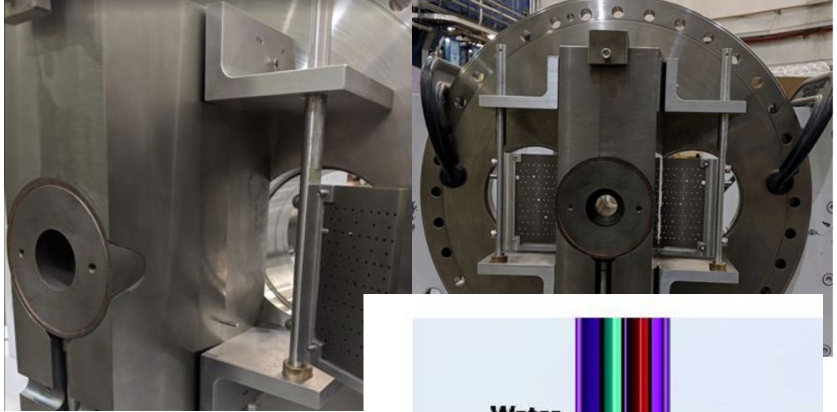

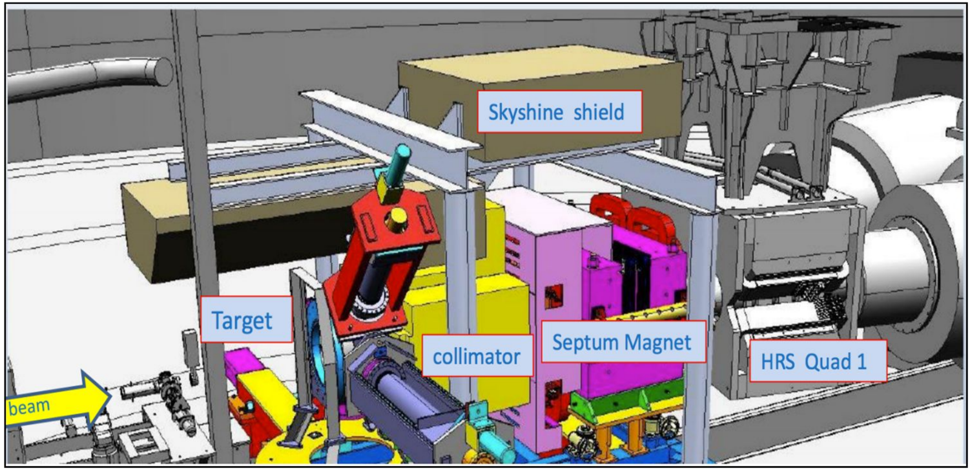

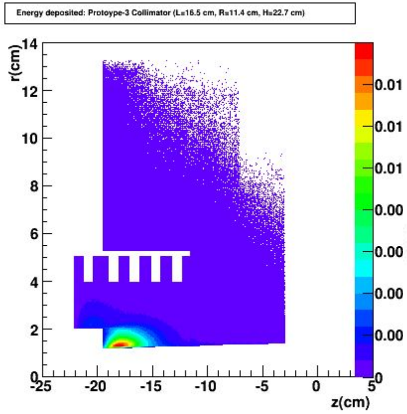

Geant4 Simulation

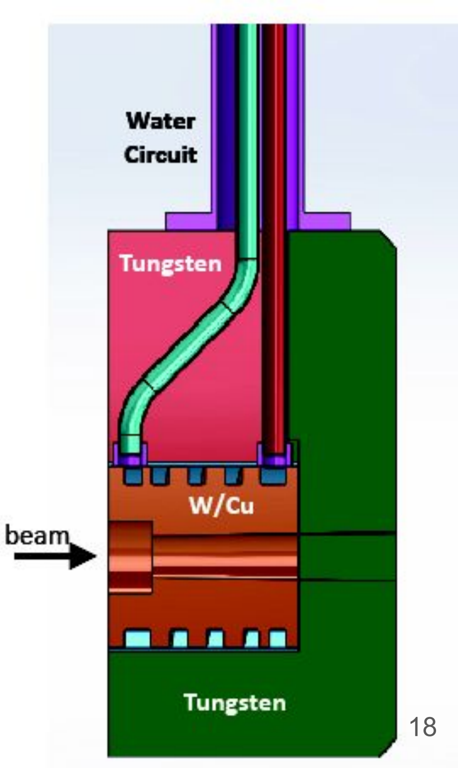

Target

- Diamond-lead-diamond sandwich targets were used to get heat out of the target to cryocooling
- Diamond eventually breaks down, and lead is damaged
- PREX-1 proved concept and demonstrated target lifetime
- For PREX-2 we prepared a complement of 10 isotopically pure targets (used 6, as expected)
- Simulations predicted approximately 72 W of power deposition from the 70 μA rastered beam

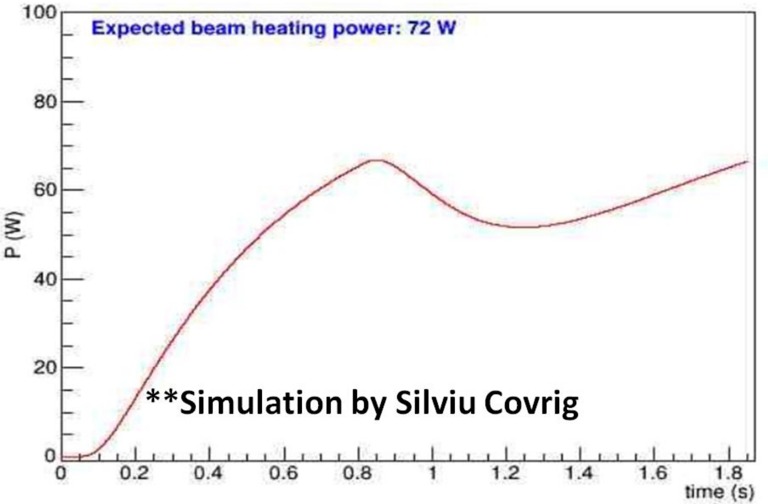

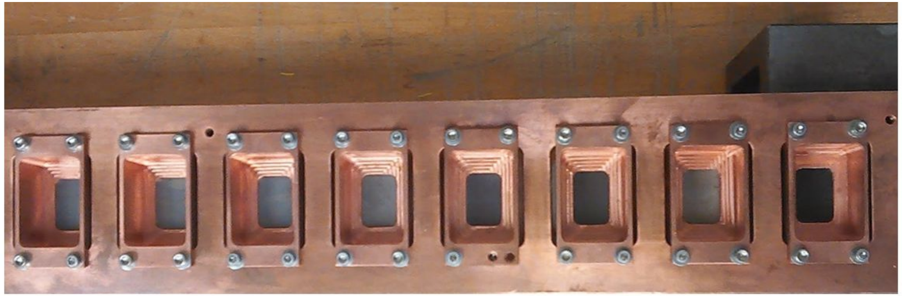

Auxiliary Target for Calibrations and Systematic Studies

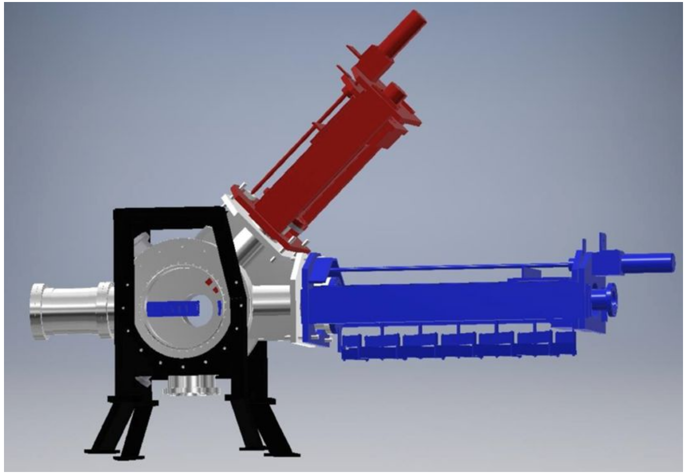

- Long horizontal target ladder
- 45^0 optics ladder
- Challenging system, successfully implemented by the target group

Integrating Detectors

- About 2 GHz signal rate in a 3x3 cm^2 area at the end of the detector
- The challenge: all electrons need to count the same - **high photon statistics but low shower fluctuations**
- Radiation hard fused silica **Cherenkov detectors** (Two in each HRS arm)
- Each one is 5mm thick, 3.5x16 cm^2 area, mated to a single PMT
- Non-linearity of detector response was tested on the bench and with beam during the experiment

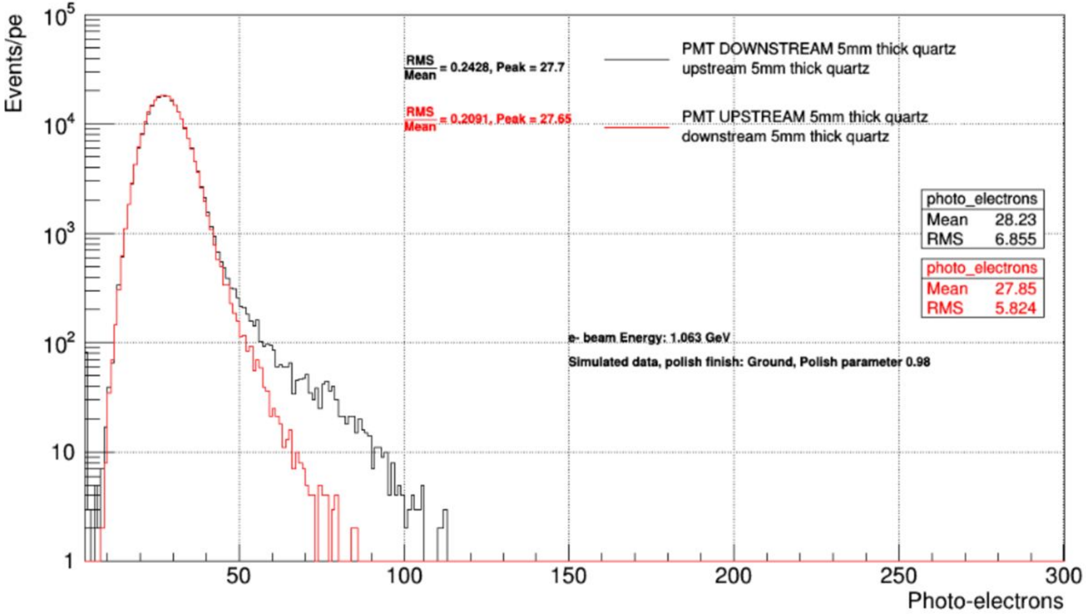

Dustin McNulty, Devi Adhikari

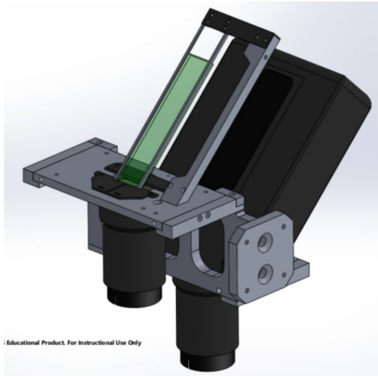

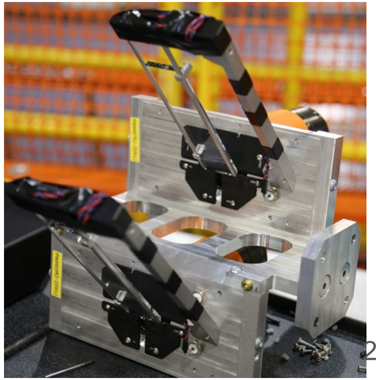

Counting Detectors

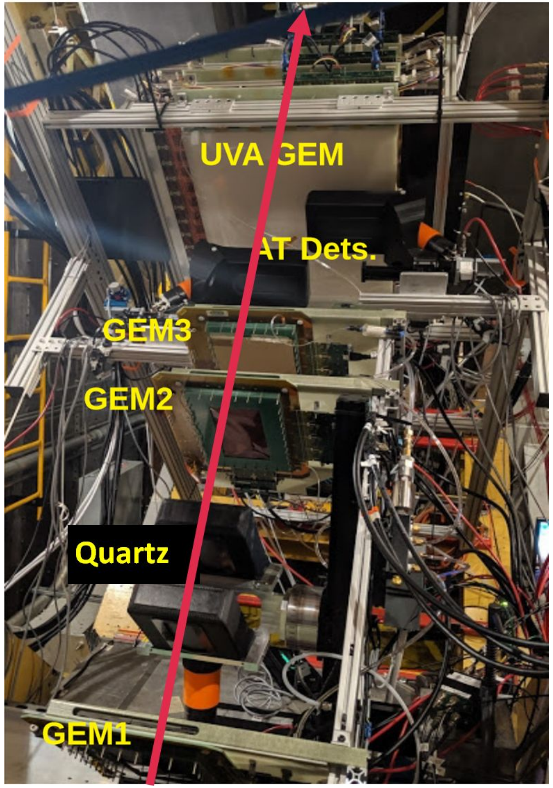

- The HRS Vertical Drift Chambers (VDCs) below the quartz detectors
- GEMs installed upstream and downstream of our quartz detectors
- Used to align the elastic peak on the quartz and to measure accepted kinematics
- Used at very low currents (30 nA) "**counting experimental mode**"

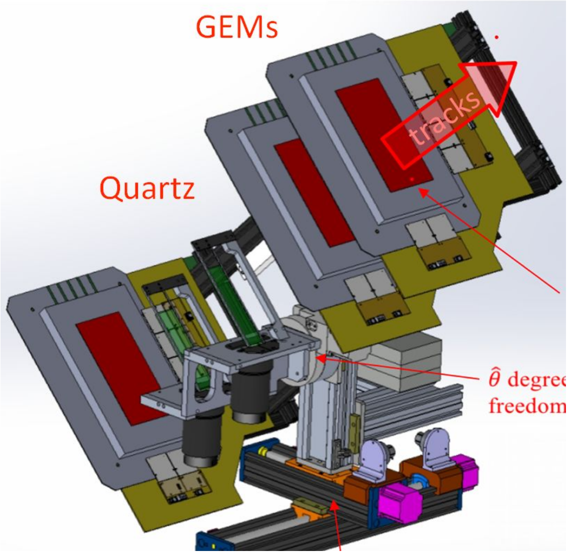

Beam Monitors and Correctors

The entire experiment setup from polarized source to the target are recorded using various detector systems in the beam line:

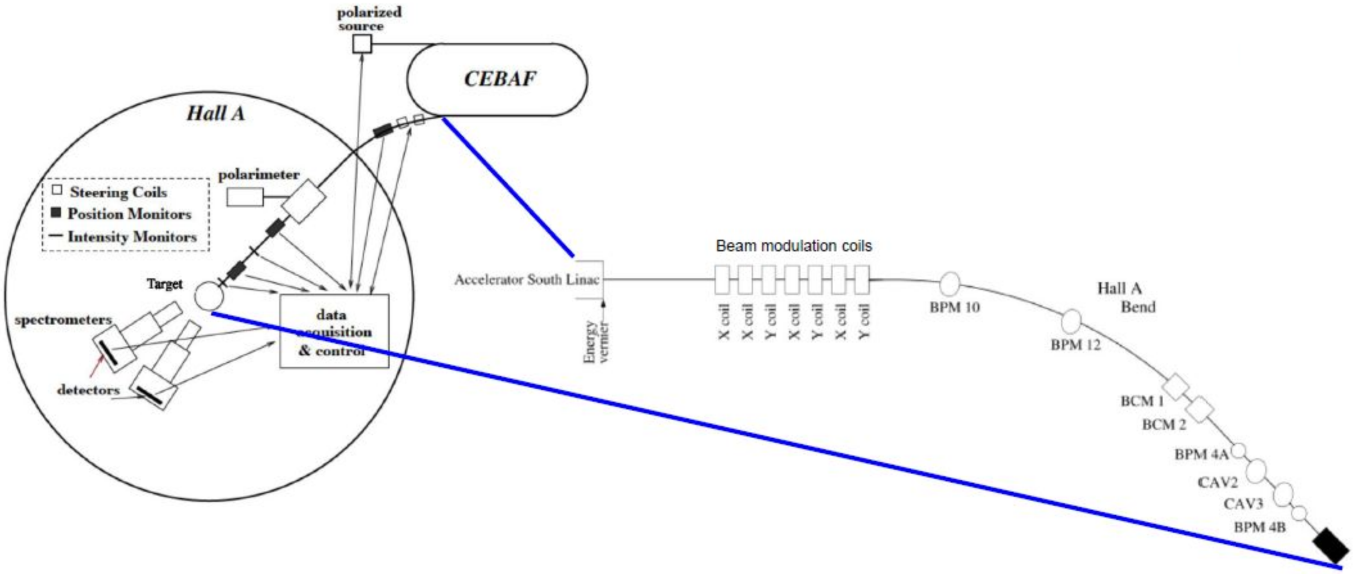

Beam Corrections

- Very forward angle: very sensitive to beam corrections.
- Beam jitter noise several times greater than counting statistics

$$A = A_{raw} - A_Q - \sum_i \beta_i \Delta x_i - \beta_E A_E$$

- Potential for systematic error if average beam asymmetries are not well corrected
- Multiple techniques used to calibrate correction factors (β_i β_E)

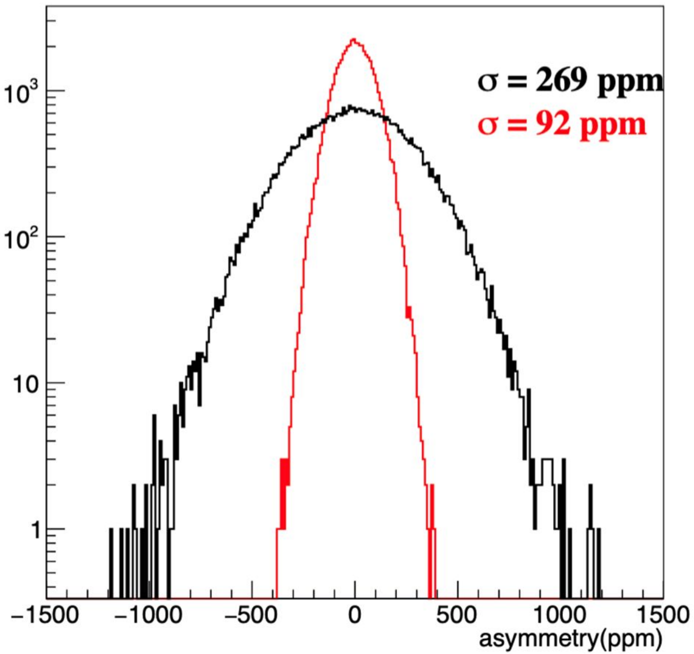

Beam Modulation (Dithering) system

- To span the 5 dimension phase space of beam motion at the target (position, angle, energy) we made use of a set of 6 coils and an energy vernier
- The extra set of air-core dipoles (coils) can be used as a cross check to confirm our procedure doesn't introduce unwanted noise
- This modulation is automated and was performed throughout the data taking period

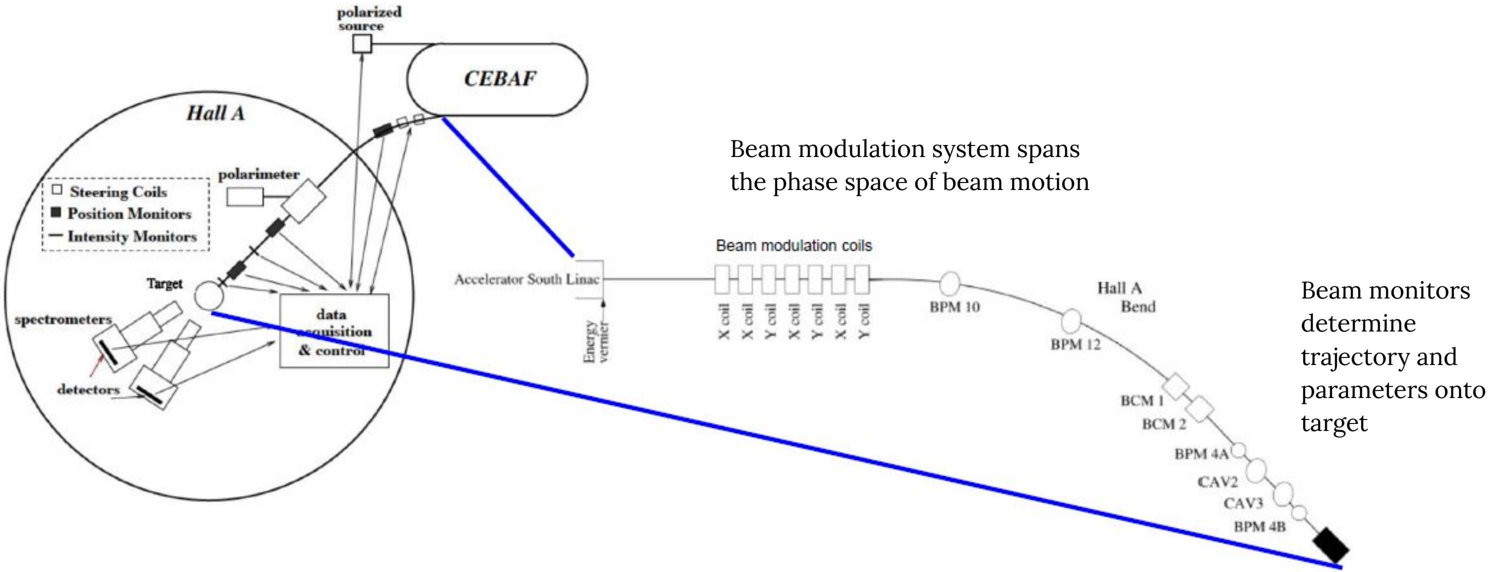

Beam Correction Techniques

Multivariate Regression:

$$\chi^2 = \sum \left(A_{raw} - \sum_i \beta_i \Delta M_i \right)^2, \quad \frac{\partial \chi^2}{\partial \beta_i} = 0$$

- χ^2 **minimization**
- Variation in β_i dominated by **'strength sharing'**
- Bias by **(anti-)correlated electronic noise**
- Slope 'diluted' by **monitor resolution**

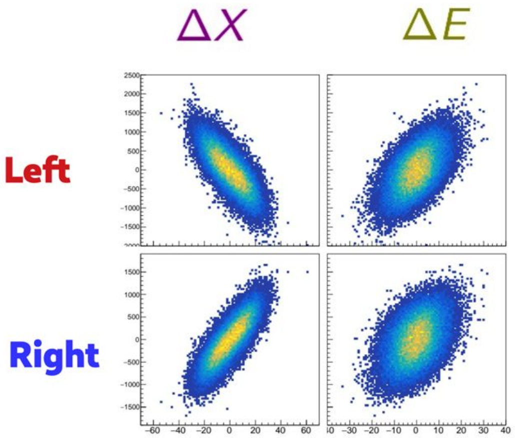

Beam Modulation:

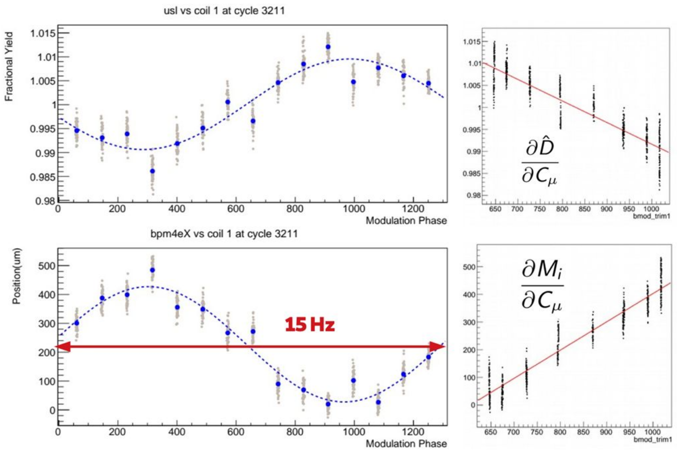

- **Modulation amplitude** $\sim$ 100 um
  - beam random jitter $<$ 10 um
  - monitor resolution 0.4 um
- **15 Hz Frequency** with repeating measurements suppresses, e.g.
  - instrumental electronic noise (60 Hz line)
  - random fluctuation in beam motion

Eigenvector Analysis and Ranking of Beam Fluctuations

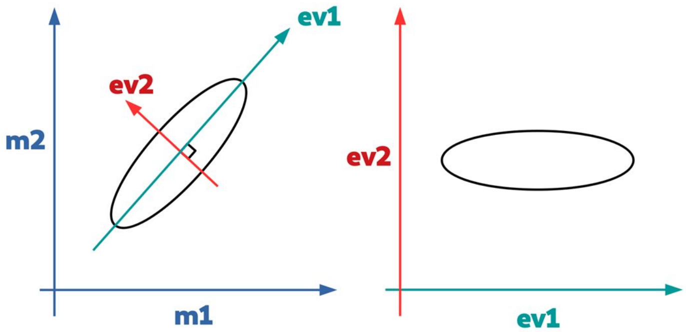

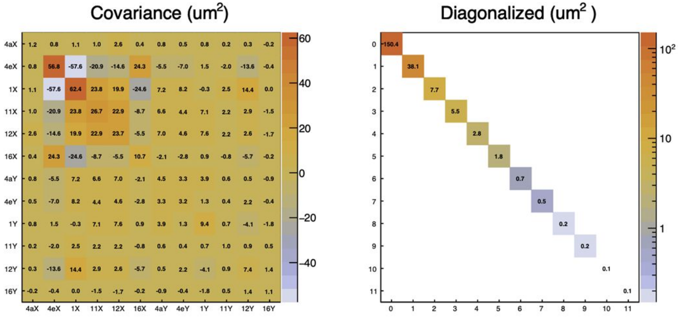

- **Diagonalize** BPMs covariance matrix $\mathcal{S}$ with eigenvalues decomposition: $\mathcal{Q}^T\mathcal{S}\mathcal{Q} = \Lambda$
- **Normalization:** $\mathcal{Q}^T\mathcal{Q} = \mathbb{I}$
- **Ranking** eigenvectors by eigenvalue $\lambda_1 > \lambda_2 > \lambda_3 \ldots$
- $\sqrt{\lambda}$ = **RMS: the ranking of beam fluctuations**

	RMS(um)
X1	14.9
Y1	9.6
E	7.0
Y2	3.3
X2	2.6
	1.3
	0.9
	0.7
	0.4
	0.3
	0.3
	0.3

Mostly BPM Electronic Noise

- Helps understand the removal of noise/bias from regression with extra beam monitors
- Assists direct comparison of beam modulation and regression techniques
- Over the course of the run, these dynamic eigenvectors retained their identification with dominance of specific beam monitors

Method of Lagrange Multipliers

- Regression precision but beam modulation accuracy
- “Hybrid" of regression and beam modulation techniques
- Assists direct comparison of beam modulation and regression techniques

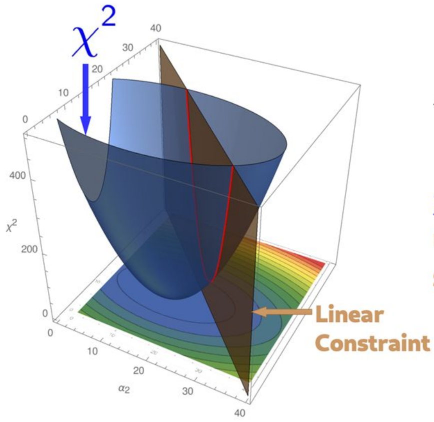

$$\mathcal{L} = \chi^2 + \sum_\mu \lambda_\mu \left(\frac{\partial D}{\partial C_\mu} - \sum_i \beta_i \frac{\partial M_i}{\partial C_\mu} \right)$$

χ^2 **minimization** with **beam modulation sensitivities constraints**:

$$\frac{\partial \mathcal{L}}{\partial \beta_i} = 0, \quad \frac{\partial \mathcal{L}}{\partial \lambda_\mu} = 0$$

Analysis chain

- **Constraint** 12 BPMs with chosen 5 coils
- **Residual Sensitivity** is checked by other 2 coils
- **Statistics** test
- **Regression** cross-check

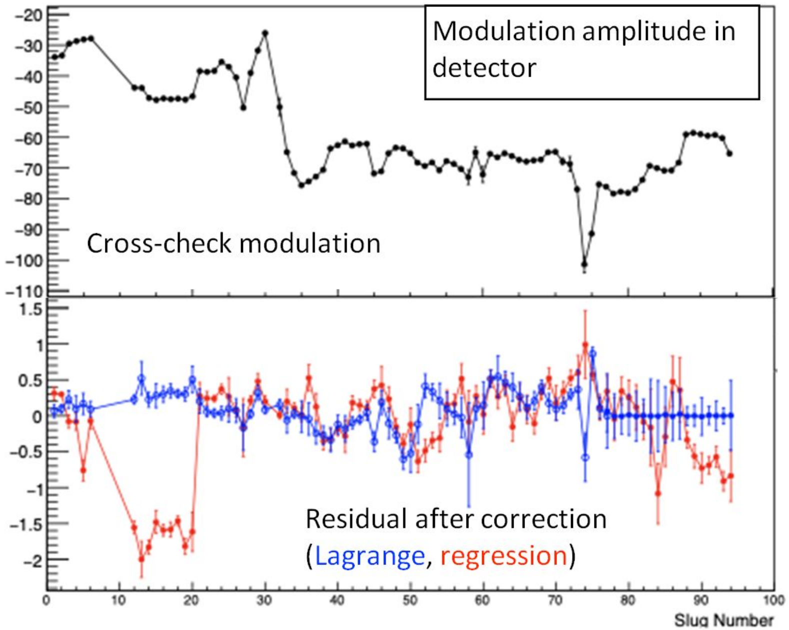

Beam Correction Summary

Three independent techniques are used and compared

1. Lagrange multiplier regression
2. regression
3. beam modulation

- Three independent techniques agree
- Use Lagrange Multiplier Regression (3% slope uncertainty)
- Left/right symmetric detectors cancel position differences
- Correction is dominated by energy jitter

type	Mean(ppb)
X1	-22.33
Y1	22.5
E	-70.44
Y2	-2.84
X2	9.7
Mostly Beam monitor Electronic Noise	1.27
	-0.01
	1.06
	0.26
	0.24
	0.18
	0.06
Total	-60.38

Total beam corrections:
(60.4 ± 2.5) ppb

PREX Data Set

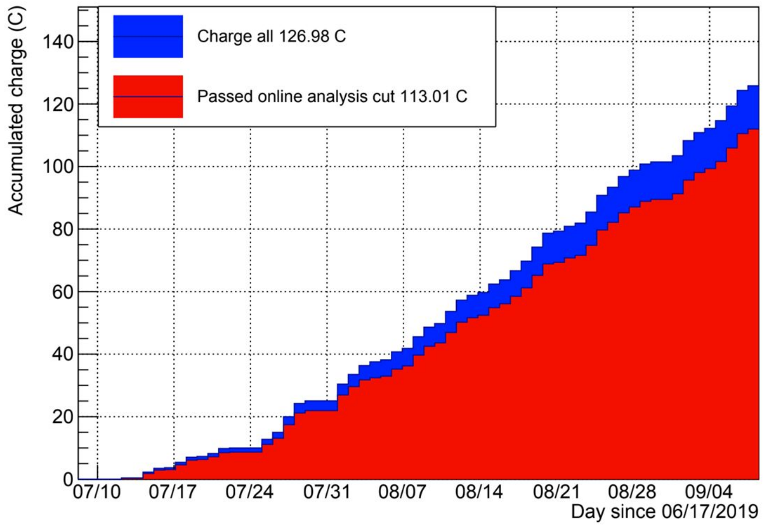

At the end of the experiment we collected about 113 C of charge on target with only about 14 C being excluded in calibrations or due to poor beam conditions (mostly, trip recovery, beam excursions, or beam monitor issues)

For our final analysis we managed to recover a bit more data ~ 114 C

Data Overview: Corrected Asymmetry

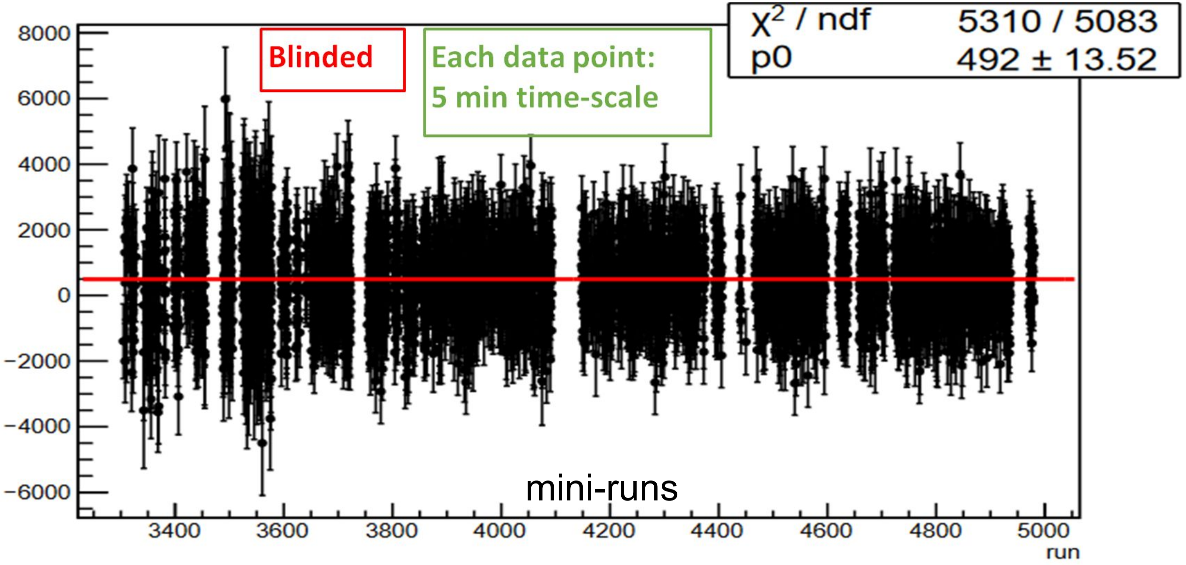

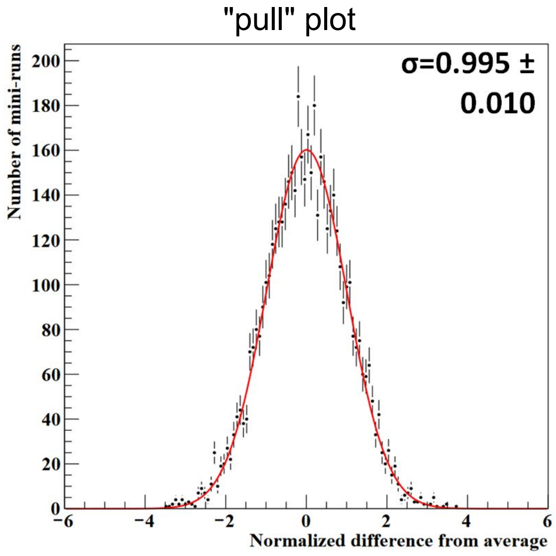

- The corrected asymmetry after effects from beam asymmetries and noise are removed
- Still to come: polarization and background corrections

Data Overview: Corrected Asymmetry

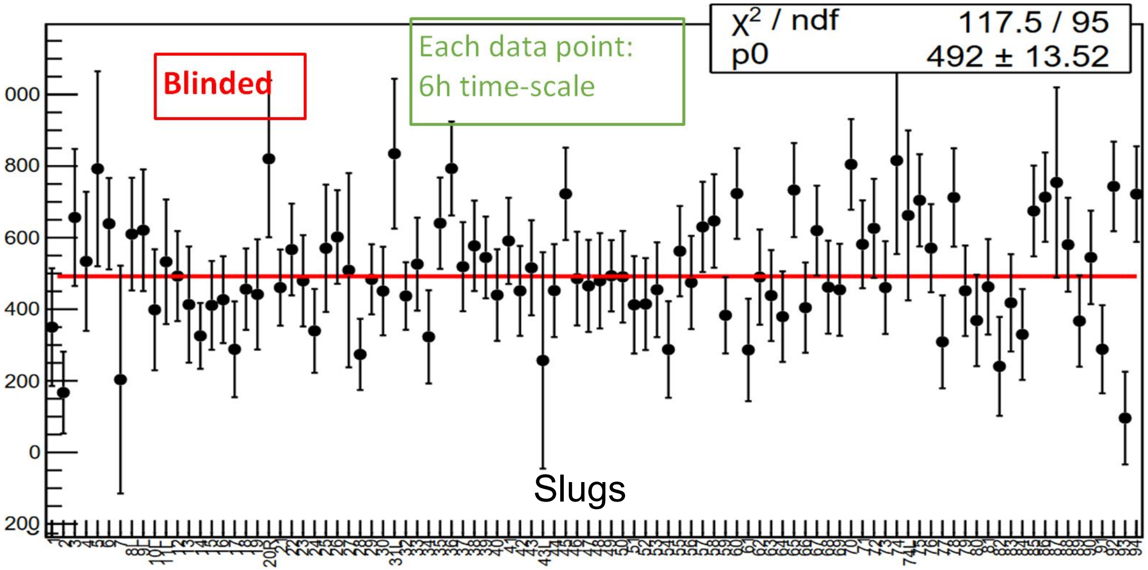

- The corrected asymmetry after effects from beam asymmetries and noise are removed
- Still to come: polarization and background corrections

Data Overview: Corrected Asymmetry

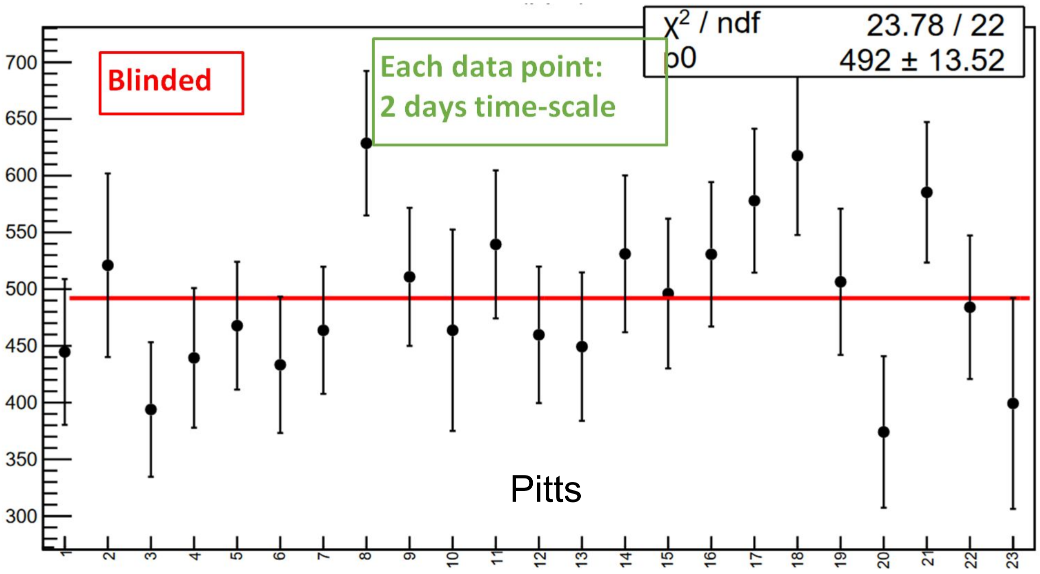

- The corrected asymmetry after effects from beam asymmetries and noise are removed
- Still to come: polarization and background corrections

Data Overview: Corrected Asymmetry

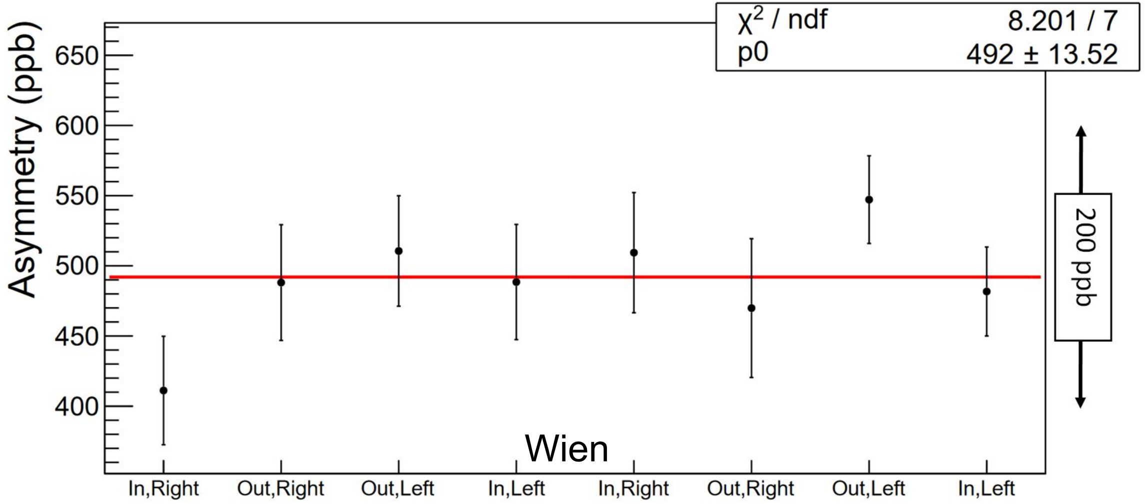

Half Wave Plate: IN/OUT
Wien: Left/Right

Total beam corrections:
(60.4 ± 2.5)ppb

- The corrected asymmetry after effects from beam asymmetries and noise are removed
- Still to come: polarization and background corrections

Null Asymmetry

$$A_{null} = \frac{A_{IN} - A_{OUT}}{2}$$

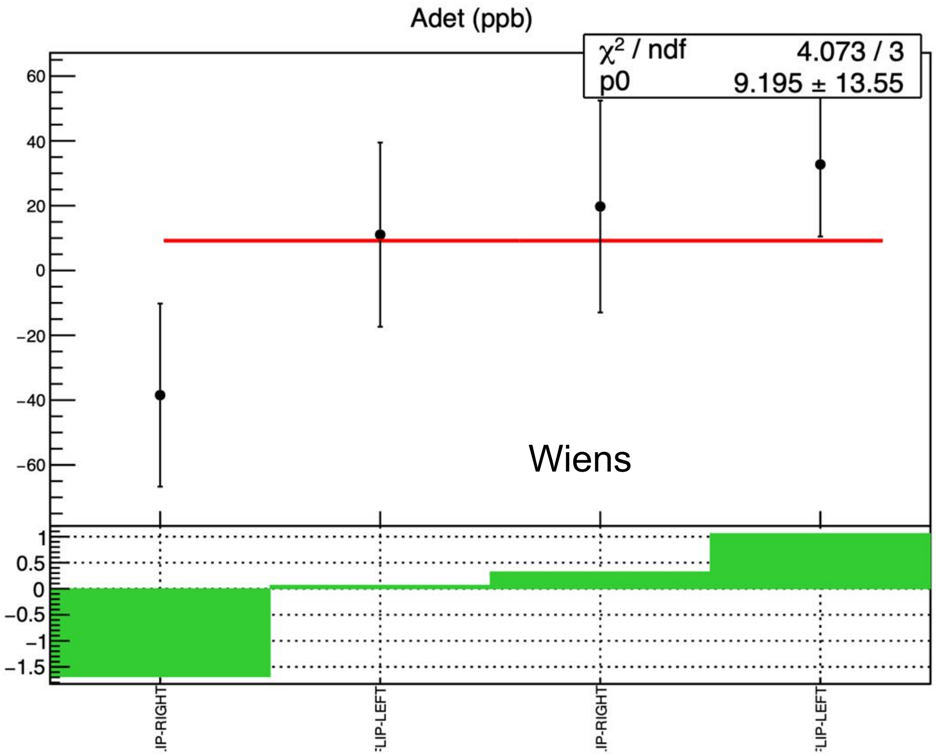

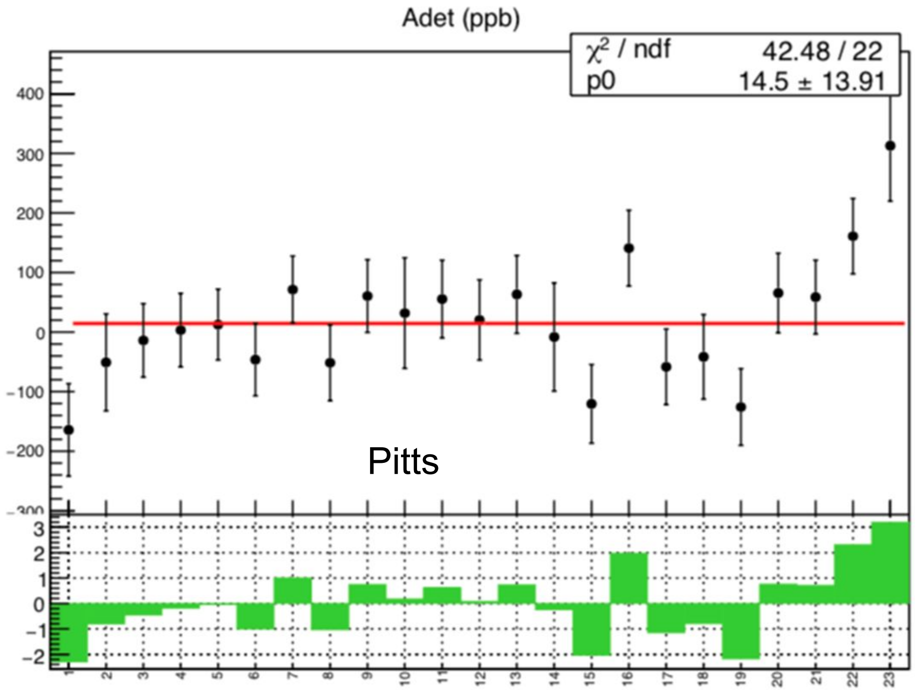

Extracting A_{PV}

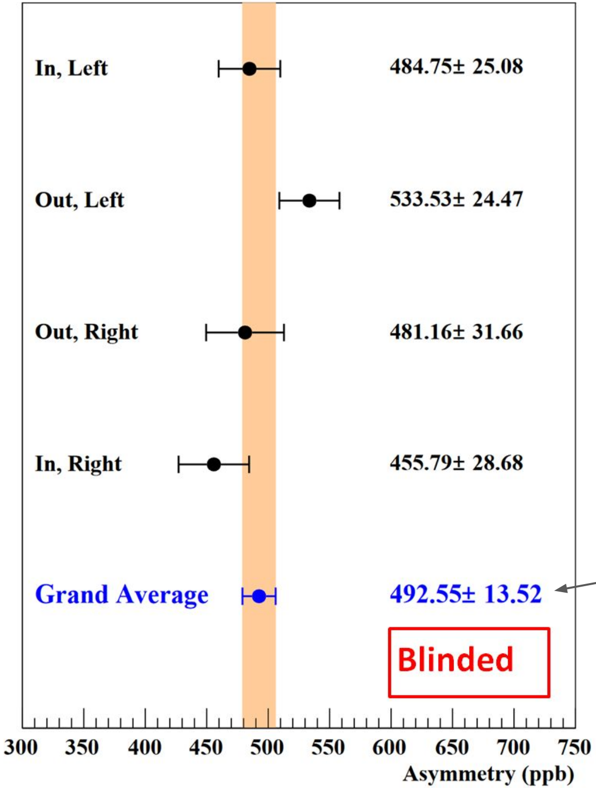

Final result averaging over all IHWP and Wien flip configurations

$$A_{PV} = R_{acceptNorm} \frac{A_{corr}/P_e - \sum_i A_i f_i}{1 - \sum_i f_i}$$

$$A_{corr} = A_{raw} + A_{beam} + A_{nonLin} - A_{blind}$$

- $R_{acceptNorm}$: Acceptance normalization
- A_{corr}: Corrected asymmetry
- P_e: Polarization
- A_i: Background asymmetry
- f_i: Background fraction

Extracting A_{PV}

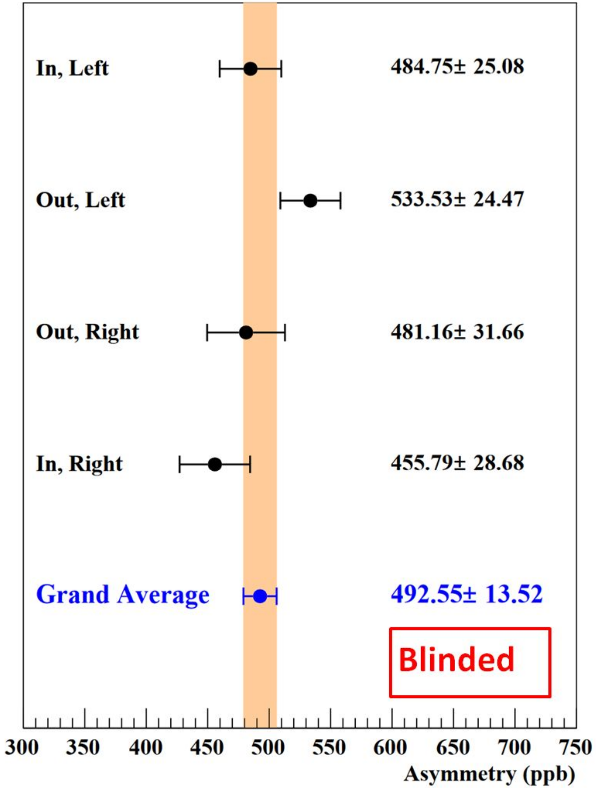

Final result averaging over all IHWP and Wien flip configurations

Blinded A_{PV}:
(549.4 ± 16.1)ppb

	A_{PV} uncertainty contribution [ppb]	A_{PV} uncertainty contribution [%]
Polarization	5.23	0.95%
Acceptance normalization	4.56	0.83%
Beam correction	2.98	0.54%
Non-linear detector response	2.69	0.49%
Carbon dilution	1.45	0.26%
Charge correction	0.25	0.04%
Inelastic contamination	0.12	0.02%
Total	**8.16**	**1.48%**

When taken all into account the experimental systematic uncertainty comes to about 1.5%

Extracting A_{PV}

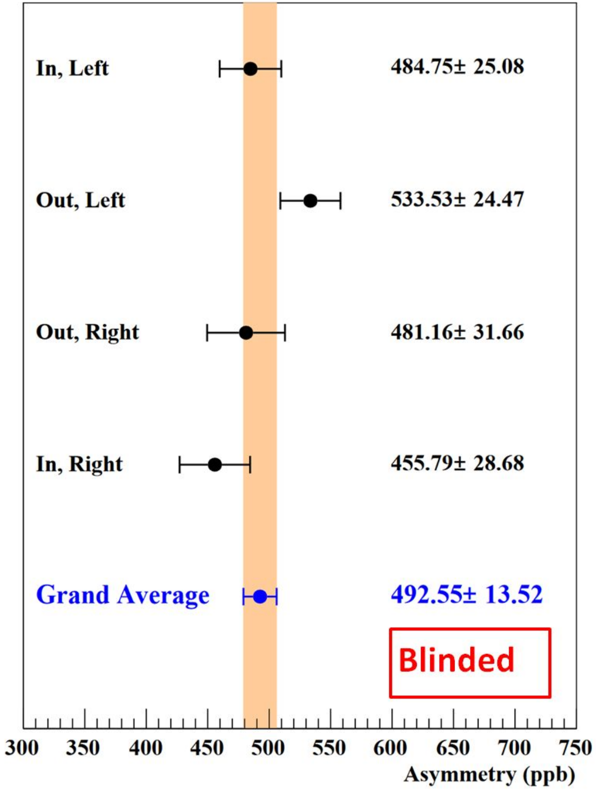

Final result averaging over all IHWP and Wien flip configurations

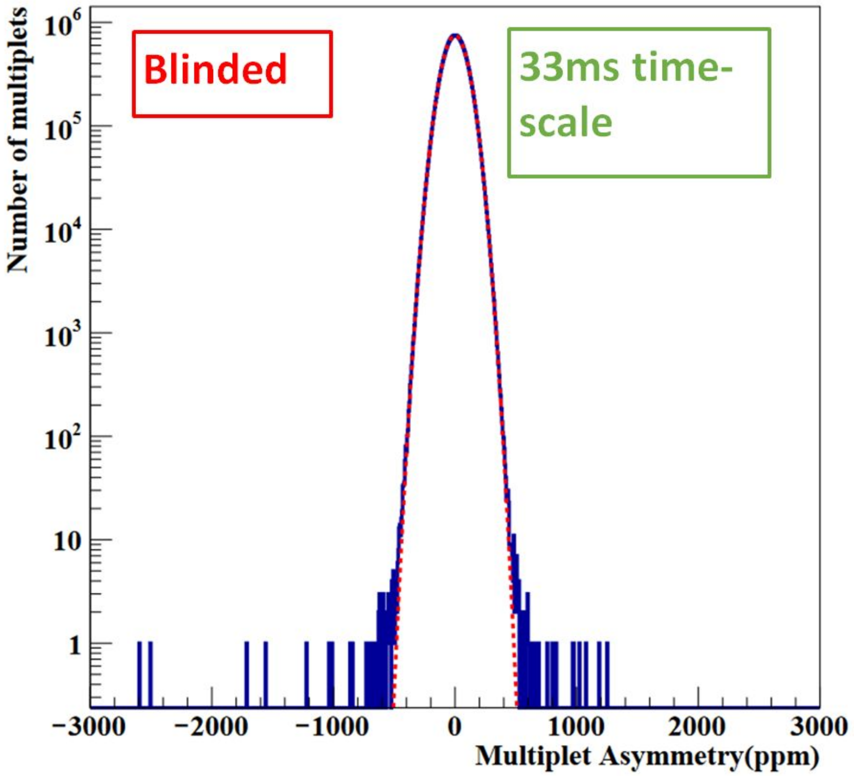

- Individual octets (70µA, 240Hz)
- Extremely consistent widths, negligible tails

Unblinded A_{PV}

“Blinding box” is ± 160 ppb: an additive term on every octet asymmetry, randomly selected (flat) at the start of the run

Blinded A_{PV}:

(549.4 ± 16.1)ppb

Blinding term turned out to be 0.5313 ppb

Unblinded A_{PV}:

(550.0 ± 16.1)ppb

Absolute angle determination and Q^2 measurement

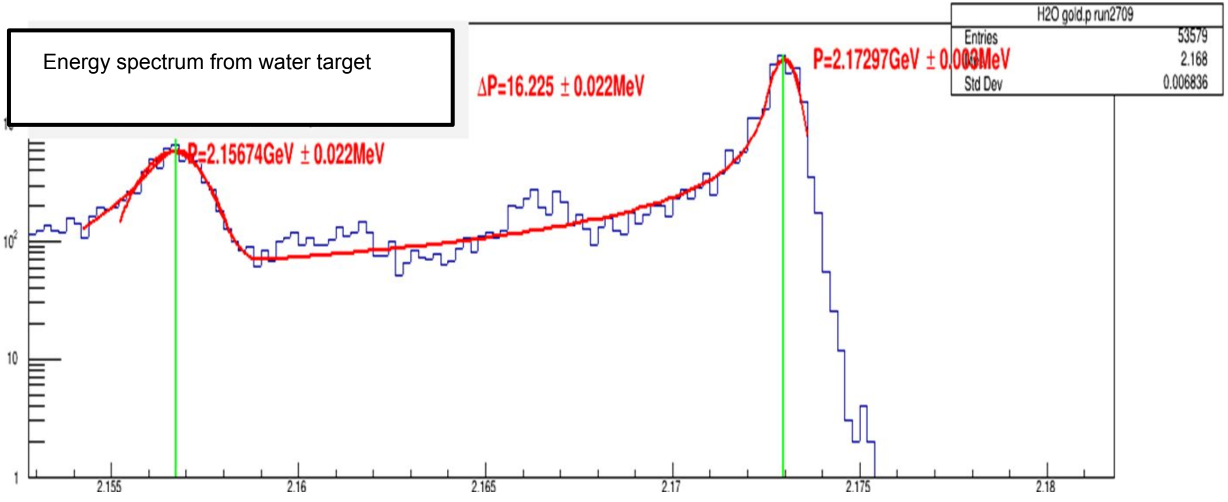

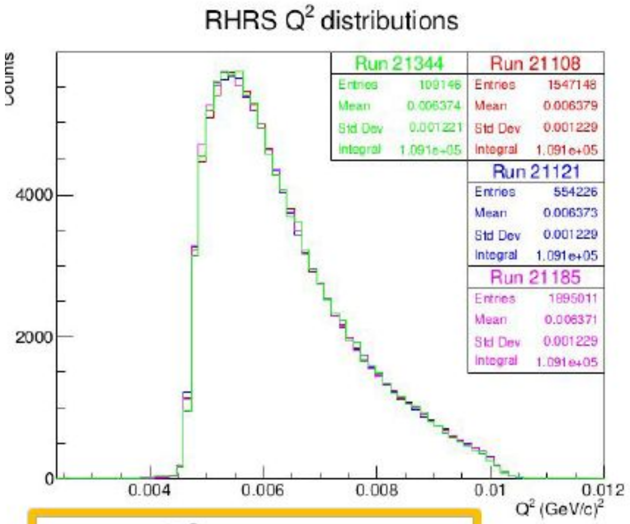

L-HRS angle:
$(4.765 \pm 0.016)^\circ$

R-HRS angle:
$(4.747 \pm 0.018)^\circ$

Q^2 average:
(0.00616 ± 0.00004) GeV^2

Absolute angles of the spectrometers are determined by measuring the recoil H and O nuclei using a watercell target.

Q^2 are measured periodically using tracking detector and no significant variation is observed

Extraction of Weak Radius and Neutron Skin

Plot the correlation between A_{PV} vs. weak radii (R_W) from a sampling of theoretical calculations*

The correlation slope is determined by fitting $\rho_W(r)$ as a 2-parameter Fermi function over a large variety of relativistic and nonrelativistic density functional models

The normalization constant in the Fermi-function form of $\rho_W(r)$ used to extract R_W is a measure of the 208 Pb interior weak density ρ^o_W

Combining with the well-measured interior charge density, the interior baryon density, ρ^o_b is determined

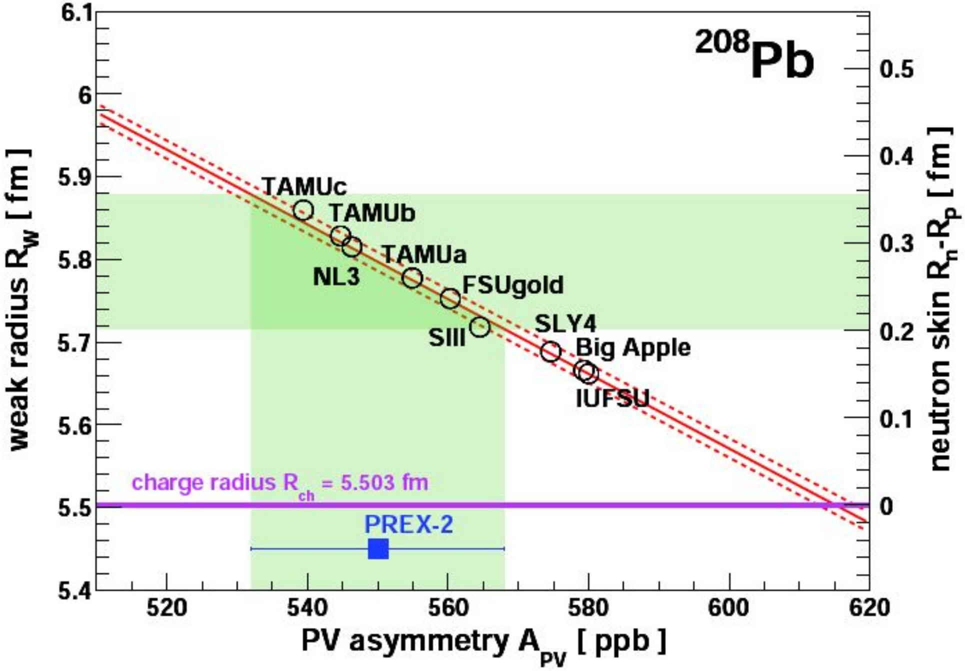

*Phys. Rev Let. 126 (17), 172502 (2021), Phys. Rev. C 102, 065805 (2020), arXiv:2007.03799 [nucl-th]

PREX Final Results

D. Adhikari et al. (PREX Collaboration)
Phys. Rev. Lett. 126, 172502
Published 27 April 2021

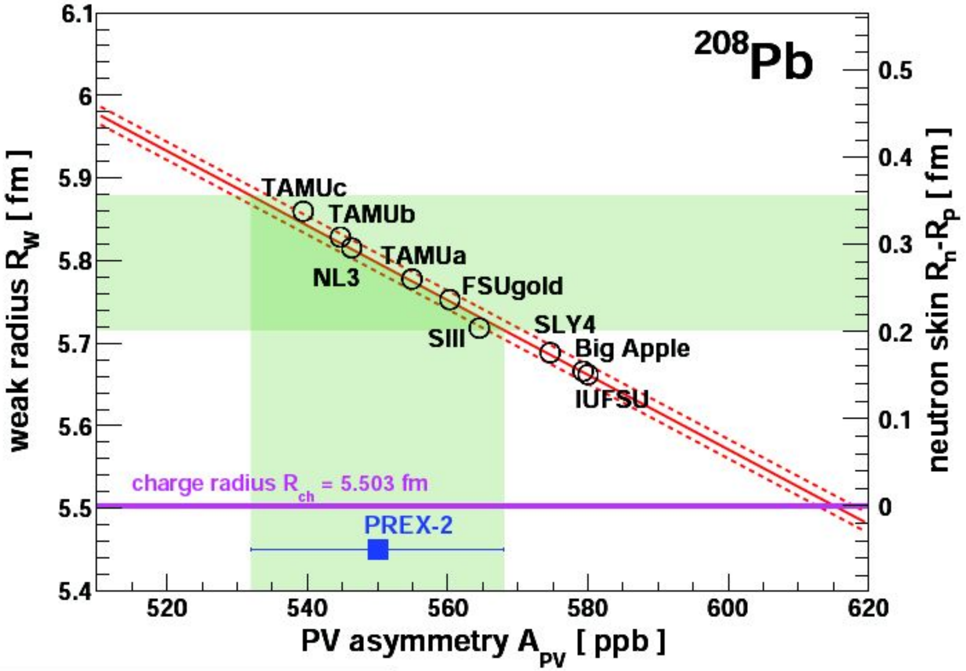

^{208}Pb Parameter	Value
Weak radius (R_W)	5.800 ± 0.075 fm
Interior weak density (ρ_W^0)	-0.0796 ± 0.0038 fm^{-3}
Interior baryon density (ρ_b^0)	0.1480 ± 0.0038 fm^{-3}
Neutron skin ($R_n - R_p$)	0.283 ± 0.071 fm

Implications of PREX

- The weak radius can be combined with the well known charge density to obtain the **baryon interior density** of ^{208}Pb
- This is the first clean determination of the **baryon interior density** of a heavy nucleus and is accurate to 2%
- Provides an important benchmark to chiral EFT calculations that is closely related to **nuclear saturation density**

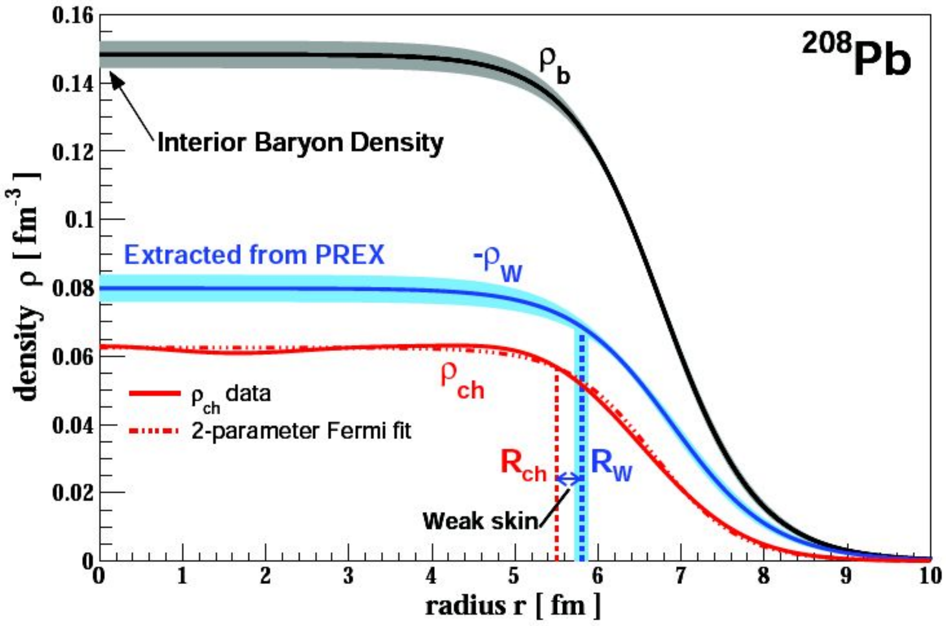

Implications of PREX

We can make use of the existing models to relate the **deformability of neutron stars** (NS) to both **neutron skin** of ^{208}Pb and to the **NS radius**. LIGO favors NS radii < 13 km

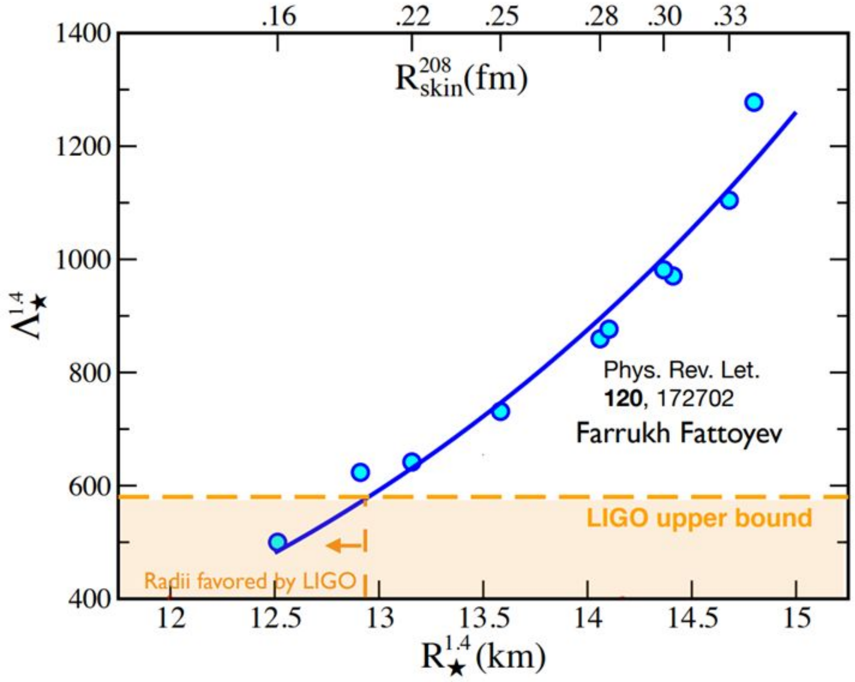

Implications of PREX

The NICER* result provides a bound on the radius of a NS

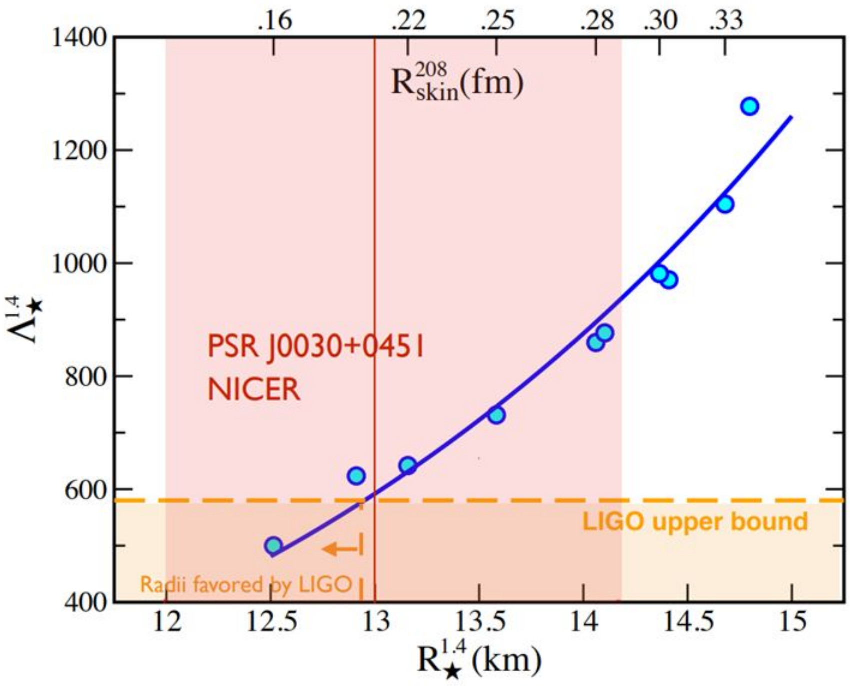

*NASA's Neutron Star Interior Composition Explorer (NICER), an x- ray spectrometer mounted on the International Space Station

Implications of PREX

- The PREX result is in good agreement with the NICER result and in slight tension with the tidal polarizability result obtained from GW170817 NS merge event observed by LIGO
- PREX Favors moderately stiff EOS (> 13 km radii)
- Consistent picture if NS radii are about 13 km

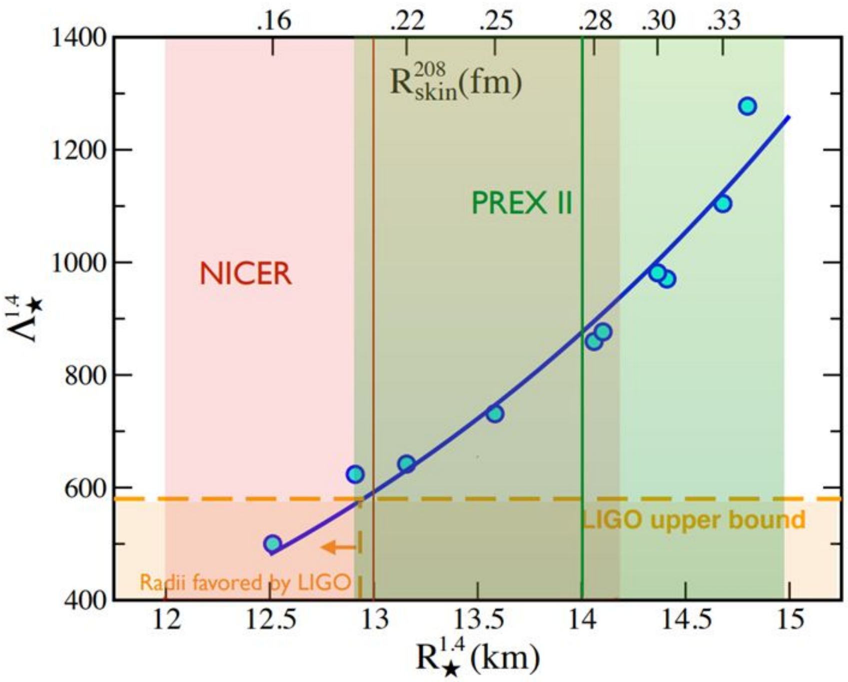

Implications of PREX: Density Dependence of Symmetry Energy, L

Exploiting the strong correlation between neutron skin and the density dependence of the symmetry energy, PREX result implies L = 106 ± 37 MeV[1] (Stiff EOS)

The expectation was about 60-70 MeV[2] (Soft EOS)

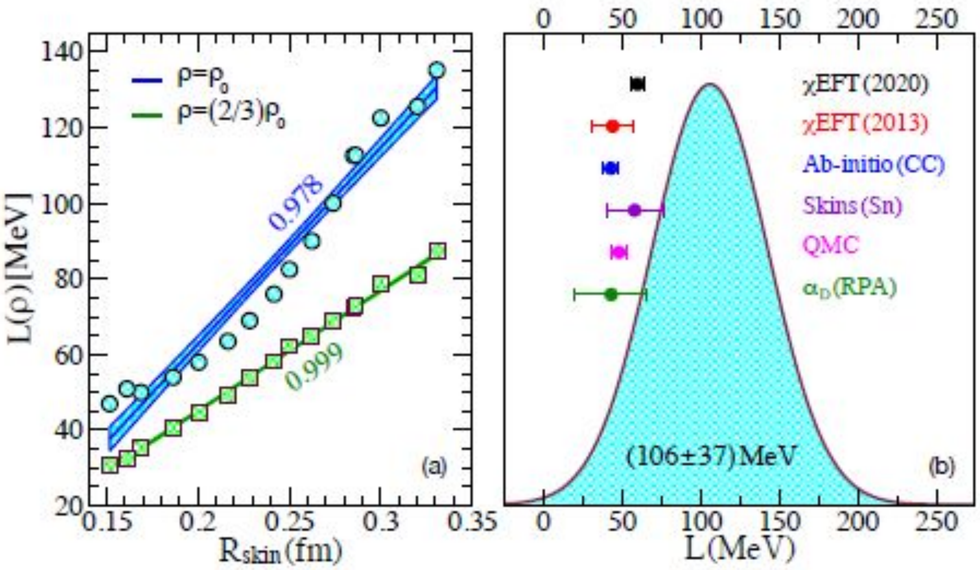

[1]B. T. Reed et. al. Implications of PREX-II on the equation of state of neutron-rich matter (2021), arXiv:2101.03193
[2]Li and Han, PLB 727 (2013), Tsang et al Phys.Rev.C 86 (2012) 015803 (2012)

Congratulations to our crew

Students: **Devi Adhikari**, Devaki Bhatta Pathak, Quinn Campagna, Yufan Chen, **Cameron Clarke**, Catherine Feldman, **Iris Halilovic**, **Siyu Jian**, **Eric King**, Carrington Metts, Marisa Petrusky, **Amali Premathilake**, **Victoria Owen**, **Robert Radloff**, **Sakib Rahman**, **Ryan Richards**, Ezekiel Wertz, **Tao Ye**, **Adam Zec**, **Weibin Zhang**





Post-docs and Run Coordinators: Rakitha Beminiwattha, Juan Carlos Cornejo, Mark-Macrae Dalton, Ciprian Gal, Chandan Ghosh, Donald Jones, Tyler Kutz, Hanjie Liu, Juliette Mammei, Dustin McNulty, Caryn Palatchi, Sanghwa Park, Ye Tian, Jinlong Zhang

Spokespeople: Kent Paschke (contact), Krishna Kumar, Robert Michaels, Paul A. Souder, Guido M. Urciuoli

Thanks to the Hall A techs, Machine Control, Yves Roblin, Jay Benesch and other Jefferson Lab staff

Special thanks to: Charles Horowitz and Jorge Piekarewicz for support and insightful conversations
Especially Chuck and grad student Brendan Reed who have worked to help us interpret our results

Supplementary

Nuclear equation of state

$$\frac{E}{A} - m = \mathcal{E}(\rho,\alpha) = \mathcal{E}_{SNM}(\rho) + \alpha^2 S(\rho) + \mathcal{O}(\alpha^4)$$

- EOS = pressure as function of density
- Energy per particle at zero temperature gives rise to the equation of state
- Laboratories help constrain EOS near saturation density $\varrho_0 \approx .150$ fm-3
- EOS is often parameterized into symmetric part and asymmetric part
- Symmetry energy describes the energy of asymmetric matter
- Expanded around saturation
- Slope parameter L strongly related to neutron skin

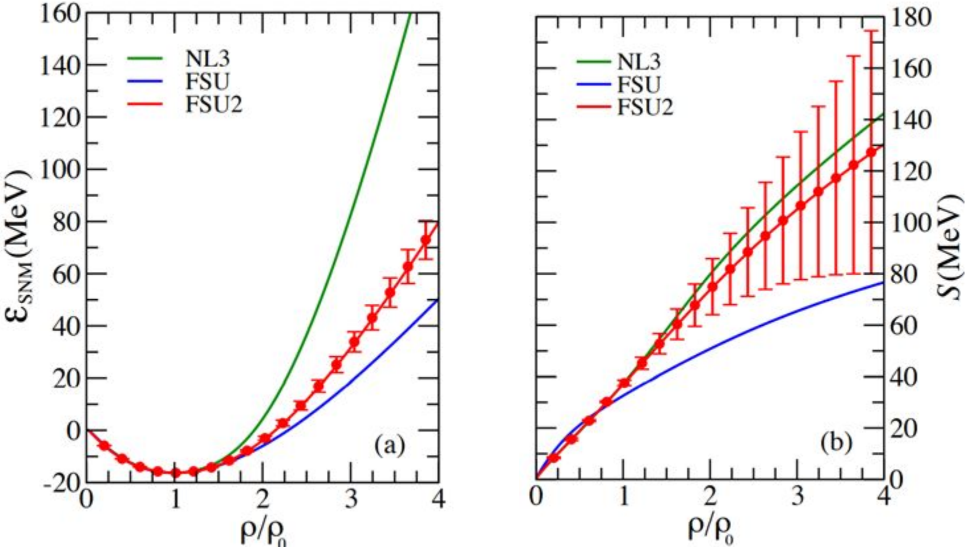

$$S(\rho) = J + L\left(\frac{\rho - \rho_0}{3\rho_0}\right) + \cdots$$

$$J = S(\rho_0) \qquad\qquad L = 3\rho_0 \frac{\partial S}{\partial \rho}\bigg|_{\rho=\rho_0}$$

Density Dependence of Symmetry Energy

Constraints on L from variety of experimental and theoretical approaches*

$$J = (38.1 \pm 4.7)\mathrm{MeV},$$
$$L = (106 \pm 37)\mathrm{MeV},$$

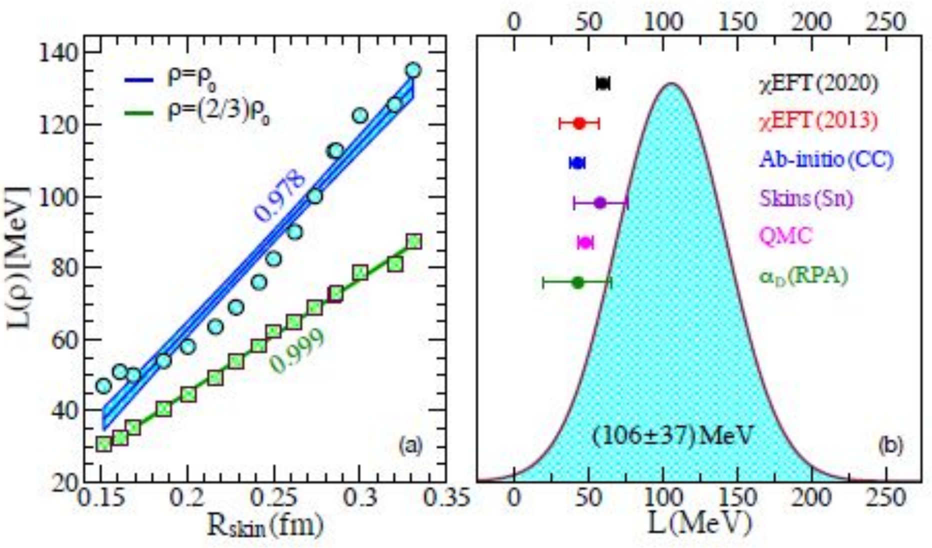

FIG. 1: (Color online) *Left*: Slope of the symmetry energy at nuclear saturation density ρ_0 (blue upper line) and at $(2/3)\rho_0$ (green lower line) as a function of $R^{208}_{\rm skin}$. The numbers next to the lines denote values for the correlation coefficients. *Right*: Gaussian probability distribution for the slope of the symmetry energy $L = L(\rho_0)$ inferred by combining the linear correlation in the left figure with the recently reported PREX-II limit. The six error bars are constraints on L obtained by using different theoretical approaches [9–16].

*B. T. Reed et. al. Implications of PREX-II on the equation of state of neutron-rich matter (2021), arXiv:2101.03193

Density Dependence of Symmetry Energy

Constraints on L from variety of experimental and theoretical approaches*

$$J = (38.1 \pm 4.7)\mathrm{MeV},$$
$$L = (106 \pm 37)\mathrm{MeV},$$

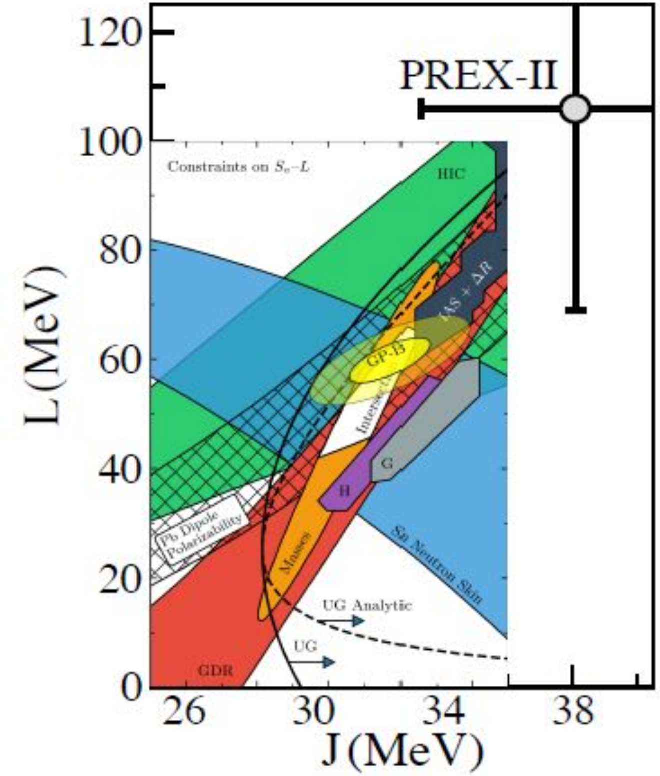

*B. T. Reed et. al. Implications of PREX-II on the equation of state of neutron-rich matter (2021), arXiv:2101.03193

Absolute Angle Calibration - Watercell

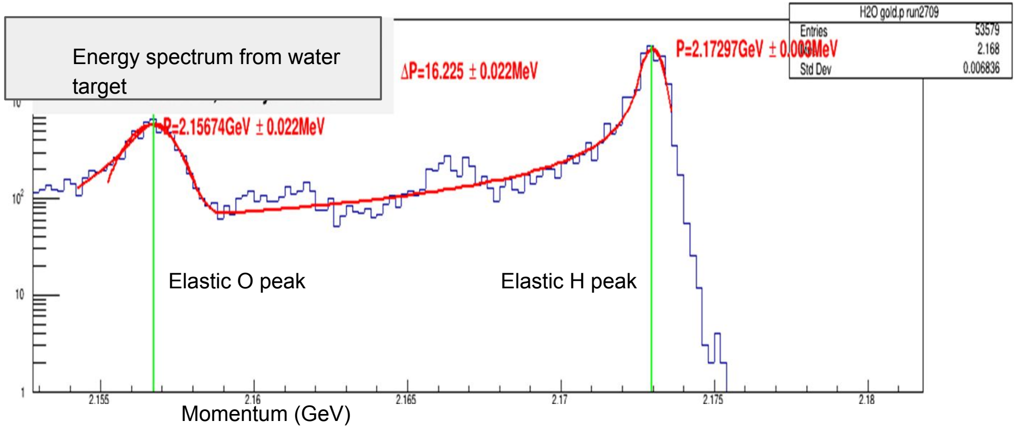

recoil momentum difference ⟶ scattering angle

- Critical to measure the absolute scattering angle to high precision
- Nuclear recoil method
- 1H and 16O in one target (same E-loss) provides straightforward measurement of angle, insensitive to other calibrations

$$A_{PV} \approx \frac{G_F \boxed{Q^2}}{4\pi\alpha\sqrt{2}} \frac{Q_W\, F_W(Q^2)}{Z\, F_{ch}(Q^2)}$$

- Determined central angle (4.76^0) to $\delta\theta = 0.02^0$
- <Q2> = 0.00616 ± 0.00004 GeV2 (δ Q2/Q2 = 0.65%)

Beam Correction Summary

- Use Lagrange Multiplier Regression (3% slope uncertainty)
- Three independent techniques agree
- Left/right symmetric detectors cancel position differences
  - correction dominated by energy

type	Mean(ppb)
X1	-22.33
Y1	22.5
E	-70.44
Y2	-2.84
X2	9.7

(Caryn Palatchi led this effort)

Δx_i	Mean (nm)	Convergence (nm)
Target x	-1.1 nm	2.0 nm
Target y	1.1 nm	0.5 nm
Angle x	-0.28 nrad	0.32 nrad
Angle y	0.14 nrad	0.09 nrad
Energy BPM	2.3 nm	1.1 nm

Total beam corrections:
(60.4 ± 2.5) ppb

Transverse Asymmetry

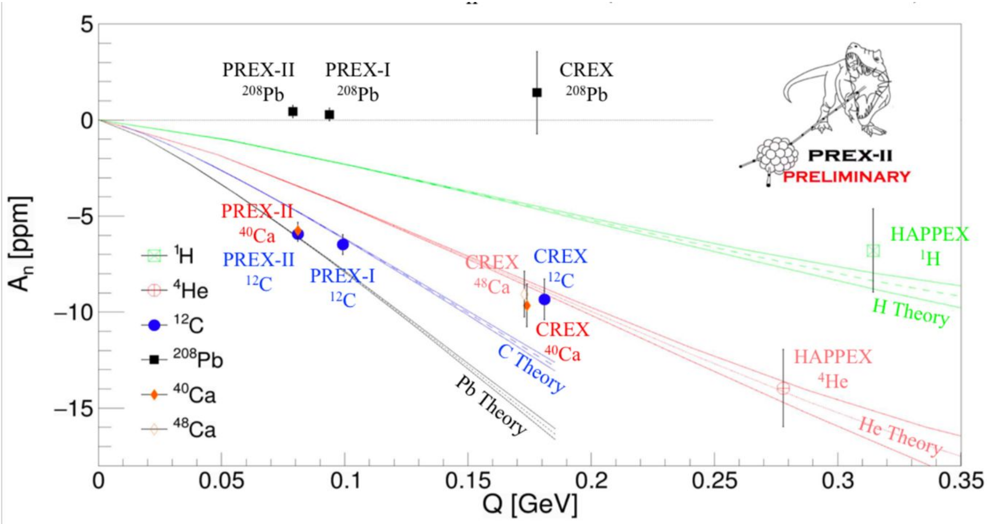

$$A_{trans} = 0 \pm 0.1 \quad \text{ppb}$$

Transverse asymmetry did not contribute a correction to the main parity violating asymmetry and the uncertainty was taken into account

Beam corrections cross-checks

Three independent techniques are used and compared

1. Lagrange multiplier regressio
2. regression
3. beam modulation (dithering)

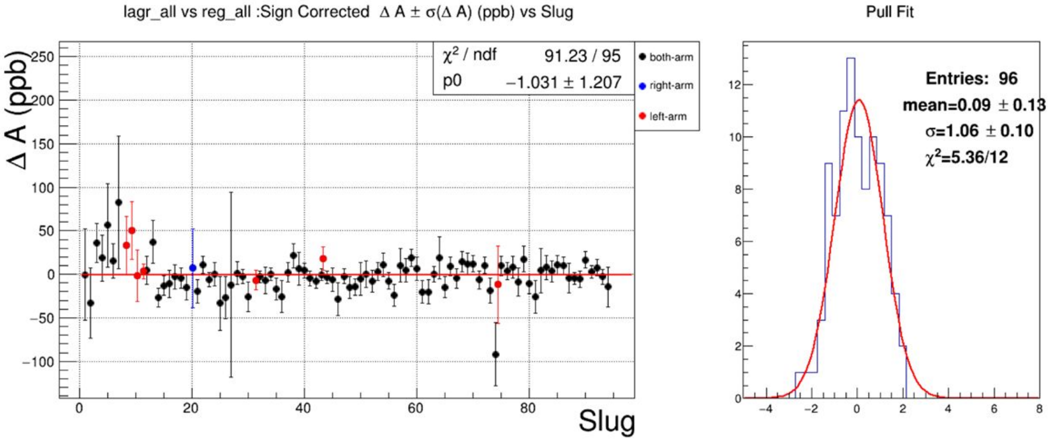

Figure: ΔA between Regression and Lagrange Multiplier by slug

	ΔA (ppb)	$\sigma(\Delta A)$(ppb)	χ^2/ndf
dit vs Lagrange	2.2	3.5	86.4 / 95
Lagrange vs Reg	-1.0	1.2	91.2 / 95

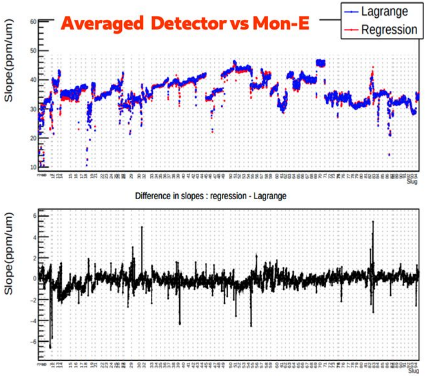

Slopes are compared:
very small (<3%) differences

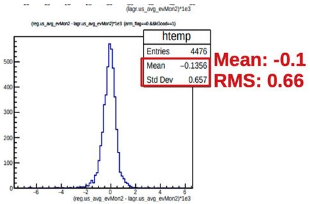

Corrections are compared over the run and seen to be statistically compatible

Method of Lagrange Multipliers

- The different correction techniques see the beam motion differently
  - We rotate the BPMs into an averaged eigenvector basis that diagonalizes intrinsic beam motion and brings slopes into agreement at few % level
- Assists direct comparison of beam modulation and regression techniques
- Uses beam modulation sensitivities to constrain regression
  - Regression precision but beam modulation accuracy

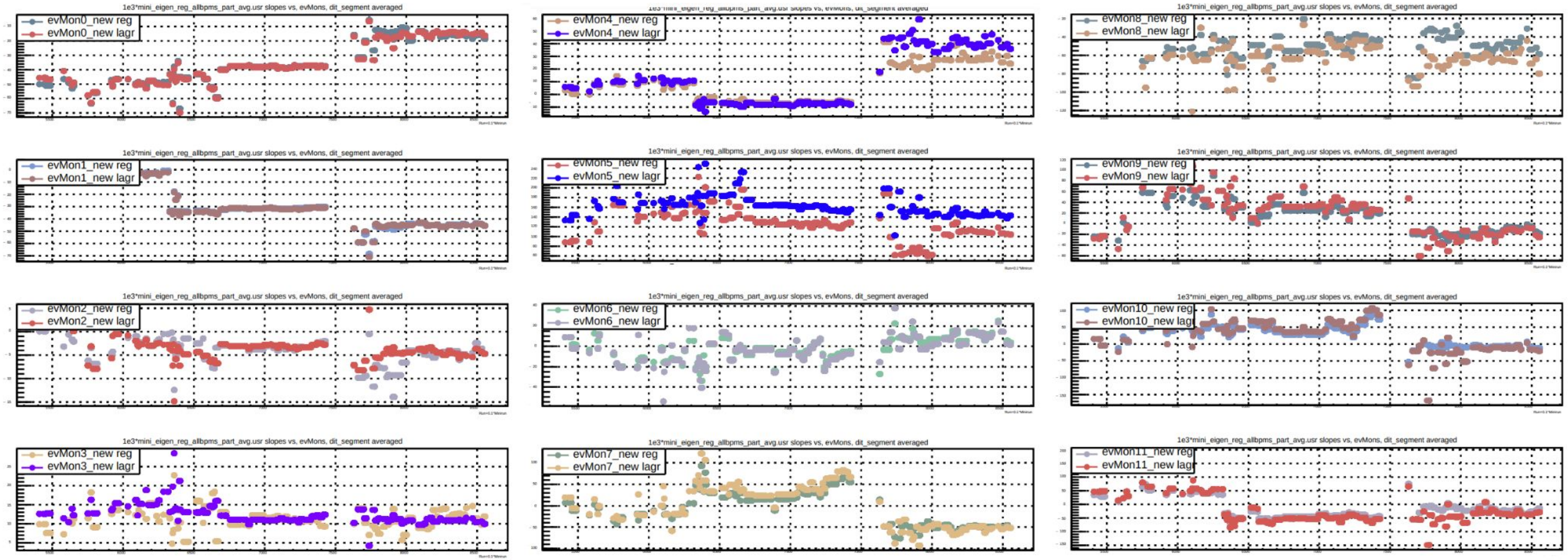

Comparison 12 BPM eigenvectors regression vs. Lagrange slopes

Electronics Radiation Damage Chart

Relative Silicon Damage vs. Neutron Energy

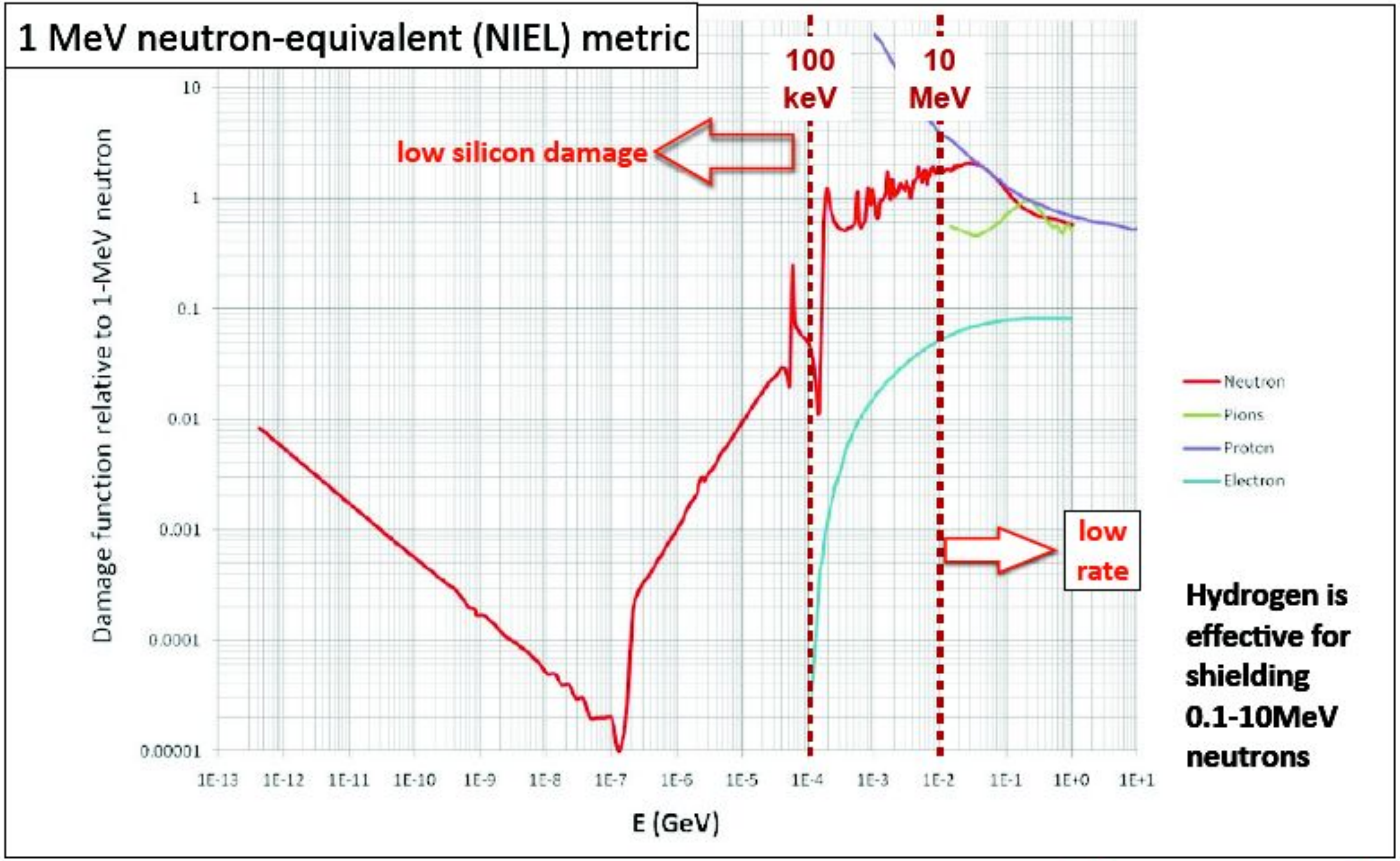

Hydrogen is effective for shielding 0.1-10MeV neutrons

Commercial off-the-shelf electronics are typically robust up to about 10^{13} *1-MeV n_{eq}/ cm^2* 3

Level required for damage expected on 'Not Radiation-Hard' electronics is 1×10^{13} (1 MeV equiv Neutron)/cm^2